Investigation of the Forces Developed when using High-Temperature Superconductors with Linear Electric Machines

Leonardo Poeti

A dissertation submitted to the Faculty of Engineering, University of the Witwatersrand, Johannesburg, in fulfilment of the requirements for the degree of Master of Science in Engineering.

Johannesburg, July 2004

Declaration

I declare that this dissertation is my own, unaided work, except where otherwise acknowledged. It is being submitted for the degree of Master of Science in Engineering in the University of the Witwatersrand, Johannesburg. It has not been submitted before for any degree or examination in any other university.

Signed this __ day of _____ 20__

Leonardo Poeti.

Abstract

The proposed research of investigating the interaction between high-temperature superconductors and linear motors is introduced. Background on levitated transportation, high-temperature superconductor applications and superconductor theory is given. An analytical model is developed for calculating thrust and levitation forces produced by 3-phase windings on a pair bulk high-temperature superconductors. Results produced by this model for a spacing of 1 pole-pitch and $\frac{1}{2}$ pole-pitch are presented. In order to verify the analytical model a prototype system is built from a linear motor primary and vehicles containing 2 rows of superconductors. Two vehicles are built with different spacing between the rows of superconductors in order to investigate the effect of their positioning, with respect to the pole-pitch, on the thrust forces produced. Measured forces on these two vehicles are then compared with predicted values showing that the model predicts the forces with less than 5% error. Problems with the analytical model are also discussed. Finally it is concluded that the model developed provides insight to the relationship between high-temperature superconductors and travelling magnetic waves, and that a 1 pole-pitch separation between superconductors produces higher forces. Recommendations for further development of the prototype system are also given.

Acknowledgements

I would like to thank Prof. Charles Landy, Dr. Malcolm McCulloch, Mr. Rupert Cruise and the entire machines research group for their guidance, advice and patience. I would also like to thank my friends and family for the encouragement and support they offered me.

In loving memory of my grandmother.
Domenica Pellegrini
(1920-2003)

"The Master in the art of living makes little distinction between his work and his play, his labor and his leisure, his mind and his body, his education and his recreation, his love and his religion. He hardly knows which is which. He simply pursues his vision of excellence in whatever he does, leaving others to decide whether he is working or playing. To him he is always doing both."
–Zen Buddhist Text

Contents

List of Figures

List of Tables

List of Abbreviations and Symbols

(a_1, b_1)	bottom left co-ordinate of left current carrying area of HTS
(a_2, b_2)	top right co-ordinate of left current carrying area of HTS
(a_3, b_1)	bottom left co-ordinate of right current carrying area of HTS
(a_4, b_2)	top right co-ordinate of right current carrying area of HTS
A_{HTS}	cross-sectional area of the HTS
$\mathbf{B}$	magnetic field vector
B_x	component of magnetic field in x-plane
B_y	component of magnetic field in y-plane
B	flux density at the HTS produced by the current in the conductor (x, y direction)
dl	conductor length into the plane
EDL	Electrodynamic levitation
EML	electromagnetic levitation
$\mathbf{F}$	force vector
F_x	component of force in x-plane

F_y	component of force in y-plane
F	force on the HTS
H^*	penetration field (H_{c2} in type-II HTSs)
H_{c2}	upper critical field for type-II superconductors
H_0	applied magnetic field
H_c	critical field
HTS	high-temperature superconductor
$I(t)$	sinusoidal current in respective coil
I	current in the conductor (linear motor coils)
I	current in the conductor
$\mathbf{J}$	current density vector
Jz	critical current density of the HTS
J_c	critical current density
k_{Ah}	integration constant for phase A (HTS pellet $\frac{1}{2}$ pole-pitch away)
k_A	integration constant for phase A (first HTS pellet)
k_B	integration constant for phase B (first HTS pellet)
k_C	integration constant for phase C (first HTS pellet)
lz	length into the plane
L	length of the HTS into the page (z direction)
LM	linear motor

LTS	low-temperature superconductor
$MagLev$	magnetically levitated
PM	permanent magnet
$\hat{\mathbf{r}}$	unit vector in direction of r
r	distance between conductor and HTS
R	radius of superconductor
T_c	critical temperature
x_0	radius of superconductor portion not penetrated by flux
$YBCO$	Yttrium Barium Copper Oxide

Chapter 1

Introduction

The prospect of using magnets and electromagnets to produce levitation and frictionless motion has been the focus of much research over the years. Since the discovery of high-temperature superconductors (HTSs), there has been a large increase of research into practical applications for this technology. The increase of critical transition temperature (Tc) to over $130K$, has captured the interest of many scientists and engineers [1].

Laboratory experiments have shown that there are numerous advantages for using HTS motors as opposed to conventional motors. These include reduction in losses, weight, size and power consumption as well as providing contact-less and low noise movement [1].

HTSs are relatively new to the field of electrical engineering and even more so to the Machines Research Group at the University of the Witwatersrand, Johannesburg. In 1999 the first project incorporating bulk superconductors and linear motors was taken on by Vandenbroocke and Zachas [2]. Whereas the principles governing the design and operation of linear motors (LMs) were well known, the introduction of superconductors was new ground, as far as expertise within the Machines Research Group was concerned. For this reason, when it came to positioning the superconductors within the levitated vehicle, much was learnt through a process of trial and error.

In 2000 it was decided by the author to take a closer look at the force relationship between the LM and the bulk HTS. The two main ways in which this relationship is examined are:

1. Derive an analytical model for determining the forces; and

2. Analyse the effect of positioning with respect to LM pole-pitch.

Ultimately the objectives of this research is to provide a better understanding of the forces experienced by bulk HTSs levitating above LMs. This is done by developing a simple method for calculating thrust and levitation forces and comparing measured forces on vehicles with different HTS positioning with respect to the pole-pitch.

In order to design vehicles making use of bulk HTSs, it is necessary to understand how optimum forces can be achieved. It is thus also necessary to get a grasp of the analytical equations governing these forces. Therefore an analytical method for calculating the thrust and levitation forces is established. This method is used to model the forces on HTSs spaced 1 pole-pitch and $\frac{1}{2}$ a pole-pitch apart. For practical design reasons a $1\frac{1}{2}$ pole-pitch spacing is used instead of a $\frac{1}{2}$ due to the small size of pole-pitch. Mathematically this proves to be have no change on expected results.

A prototype system is set up and experiments are performed in order to compare two vehicle designs with different HTS positioning. The experiments entail determining how the measured thrust force is related to the operating parameters of the motor, such as voltage and current. Force measurements made on this test track are then correlated with calculated results obtained from the analytical model developed.

This report will give background information on some of the important characteristics of HTSs that were thought to be most relevant to the scope of the research. A description of the "Bean Critical State Model" for superconductors is given as this theory forms the basis of the analytical approach taken. Details of the analytical model and resulting theoretical predictions are then provided. The experimental setup is described and details of the experiments performed along with the measured results are given. Finally theoretical and measured results are compared, conclusions drawn and recommendations for further research are proposed.

Chapter 2

Background and Superconductor Theory

Since its invention in the early 1800s, the locomotive has been one of the major workhorses of industry and a main means of transportation for the masses. With the introduction of automobiles and aeroplanes, the popularity of trains as a means of transport for the masses decreased. By the middle of the 20th century, with the increasing numbers of planes and automobiles, a trend towards congestion was evident.

It should be pointed out that this progression applies more to first world countries than South Africa as the development of public transport systems in South Africa has been very slow as far as trains are concerned. Only in the last three years has there been a renewed interest in improving the train system with the Gauteng SDI Rail Link Project. According to their research,

> "*No new rail lines have been built in the last 15 years and the rolling stock is on average more than 30 years old [3].*"

In the 1960s countries like America, Germany, France and Japan initiated a drive to find faster more efficient means of ground based mass transportation. This initiative lead to three major developments [4]:

1. Improved "steel wheel on rail" trains capable of reaching speeds between 200 and 300 km/hr;

2. Controlled electromagnetic levitation (EML); and

3. Electrodynamic levitation (EDL) using low-temperature superconductor (LTS) wire.

Various reasons promoted the magnetically levitated (MagLev) trains over conventional trains, such as higher speeds with less vibration i.e. less noise and more comfort. After 20 years of development MagLev trains had reached the stage where full scale working models have been built, capable of reaching speeds in excess of 500 km/hr.

However, the peak of these low-temperature superconducting wire based MagLev technology coincided with the discovery of new high-temperature superconductors (HTSs). LTS wire is superconducting at temperatures below 10K and requires the use of liquid helium (4.2K) for cooling. HTSs become superconducting at temperatures below 90K meaning that liquid nitrogen (77K), which is cheaper and easier to produce, can be used as a coolant. This lead to much speculation of capabilities and new applications of HTS materials such as Yttrium Barium Copper Oxide (YBCO).

Initially differing views on the use of HTSs in MagLev were expressed. American MagLev designers claimed that LTSs could not be outdone by HTSs whereas Japanese authorities on the subject said that they would recommend the use of HTSs once the initial problems with these materials had been overcome. This was largely due to the brittleness and poor current carrying capacity of the first HTS materials produced [5]. Progress in the production techniques of HTSs over the last eight years has lead to new materials with higher current densities, transition temperatures and longer wire lengths [4].

Even though progress is being made in the construction of HTS wire, a good deal of research is being focused on the application of HTSs in their bulk form to produce simple and passive levitation. This applies not only to large scale devices such as trains [6] and linear electromagnetic launchers, but also small scale frictionless bearings for both rotary and linear motion. In particular there is a large interest in no-contact horizontal motion devices such as those used in electronics manufacturing for transporting silicon wafers[7] or in linear motion actuators [8, 9].

The main advantages of a levitated transport medium stem from the fact that there is no contact or friction between vehicle and track which means [4]:

- Lower maintenance;
- No dust produced;
- Higher speeds attainable; and
- No noise.

Added advantages of a passive levitation system are:

- No electronics or power supply needed on vehicle;
- Higher reliability due to low complexity; and
- Lighter and cheaper vehicle.

Whether for large scale or small scale applications, there is definitely interest and value in the possibility of a levitated medium. HTSs can achieve passive and stable levitation because of their diamagnetic and flux pinning properties [10].

2.1 Bulk HTS Applications

2.1.1 Hysteresis and Reluctance Motors

Much research has gone into the use of bulk HTS materials in order to improve rotor design and performance of hysteresis and reluctance motors. Kovalev et al [11] state that these types of HTS machines have mass-dimensional quantities 3-5 times better than their conventional counterparts. Also the specific output power of liquid nitrogen cooled HTS machines is shown to be greater than that of conventional electric machines [11]. Research done by Oswald et al [12] concur with these findings and attribute the improvement to the large amount of force density referred to the rotor surface in HTS machines. Force

densities in the order of 5 N/cm^2 are achieved with HTS reluctance motors as compared with similar standard asynchronous (1.5 N/cm^2) and synchronous (2.5 N/cm^2) motors [12].

In order to improve on the performance of the reluctance motor, it is necessary to increase the field gradient at the pole edges. In HTS materials this can be achieved by an increase in the field repelling current density. Thus a better quality superconductor will produce larger forces [12]. Hysteresis motors, on the other hand, make use of the fact that HTSs experience hysteresis losses when placed in a changing magnetic field. Barnes et al [13] have done extensive research and analysis on HTS hysteresis machines, showing that hollowing out and segmenting the rotor increases the effective usage of the HTS material. Research done by Habisreuther et al [14] on hysteresis motors with YBCO rotors, also shows that a significant increase in power output can be achieved by using better quality superconductors. Furthermore they claim a factor of 10 increase in power per motor volume compared to conventional hysteresis motors.

2.1.2 Magnetic Bearings and Linear Actuators

Calculation of levitation forces between bulk HTSs and permanent magnets (PMs) is the focus of many researchers, specifically with the aim of optimising the performance of magnetic bearings and linear actuators. Zeisberger et al [15] develop an analytical model for determining the levitation between a PM and a HTS. The premise of their research is that if the current density (J_c) tends to infinity then the force between the HTS and the PM is the same as between a PM and its image [15]. The outcome of this analysis showed that levitation forces are dependent on the critical current density and the dimensions of the specific superconductor. A similar analysis is undertaken by Chen et al who use an empirical method for calculating levitation between PMs and field-cooled HTSs. Their approach entails directly measuring the magnetic fields of both the HTS and the PM with a Hall probe. The corresponding currents required to produce such a field are then calculated and the forces between these currents are determined [16].

Here too there has been an interest in how the quality of the HTS affect

levitation forces. The quality of the HTS is largely determined by the technique used to produce the compound material. Chen et al [17] compare the levitation abilities of YBCO samples prepared by two different techniques, namely melt-textured and sintered. The melt-textured samples proved to be capable of levitating 2-3 times more weight than the sintered ones [17].

Details on HTS production methods are beyond the scope of this project, but it should be noted that the bulk HTSs used for the experimental portion of this research are melt-textured. The topic of field-cooling, where the HTS is cooled down to below its critical temperature in the presence of a magnetic field, is discussed in more detail in section 6.2.

2.2 Properties of HTSs which Affect Levitation Forces

Various intrinsic properties of superconductors can directly affect the levitation forces produced [18]. For instance: in order for an HTS to remain in its superconducting state, three critical conditions must be met. Critical temperature (T_c), critical field (H_c), and critical current density (J_c) determine the limits of the superconducting state but each one is very dependent on the other two. Thus, for a material to remain superconducting, all three properties must be below critical values. Since the three parameters are interdependent, they can be plotted against each other to form a phase diagram as in figure 2.1 [19].

The upper limits of T_c, H_c and J_c form a critical surface. Figure 2.1 shows that at 0 K[1] maximum values for H_c and J_c occur, while the peak value for T_c occurs when H_c and J_c are zero. Typical values for YBCO would be $T_c = 93\ K, J_c = 10^7 A/cm^2$ and $H_c = 250T$. It should be noted that the maximum values of T_c, H_c and J_c differ for different superconducting compounds. At the time of print the compound with the highest T_c value of (138 K) at ambient pressure, was $Hg_{0.8}T_{10.2}Ba_2Ca_2Cu_{308.33}$. For most practical applications of bulk type-II superconductors one would ideally like to maximise all

[1] Temperatures on this scale are called kelvins, NOT degrees kelvin, kelvin is not capitalized, and the symbol (capital K) stands alone with no degree symbol.

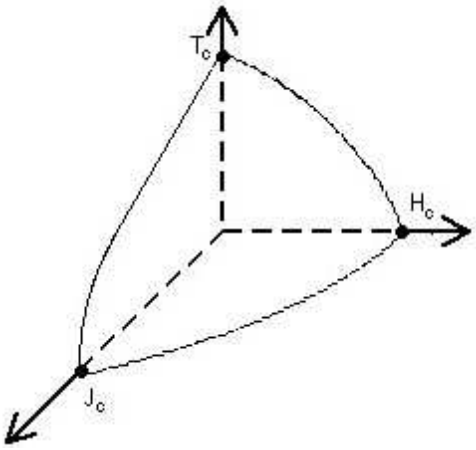

Figure 2.1: Critical Surface Phase Diagram

three variables. Thus a compromise is necessary in order to operate within the conditions of the critical surface.

Levitation forces are affected by the running conditions of the stator section and also by a number of properties specific to the superconductors. These include operating temperature, applied magnetic field and physical dimensions [18].

2.2.1 Dimensions of HTS Pellets

It has been shown that levitation forces experienced by cylindrical HTS pellets increase with increasing thickness and radius until saturation points are reached [20, 21]. Lugo and Sosa [20], and Sagar et al. [21] took two different approaches in order to derive an expression relating the force to thickness and radius. Whereas Sagar et al. solved Maxwell and London equations to derive their expression, Lugo and Sosa considered the problem as a continuous distribution of dipole-dipole interactions.

Although their approaches were different and the final expressions differed slightly, a clear relationship between levitation force, thickness and radius is shown. Figure 2.2 (a) and figure 2.2 (b) show levitation force as a function of thickness and radius respectively.

These figures show only the relationship between force and the HTS dimensions

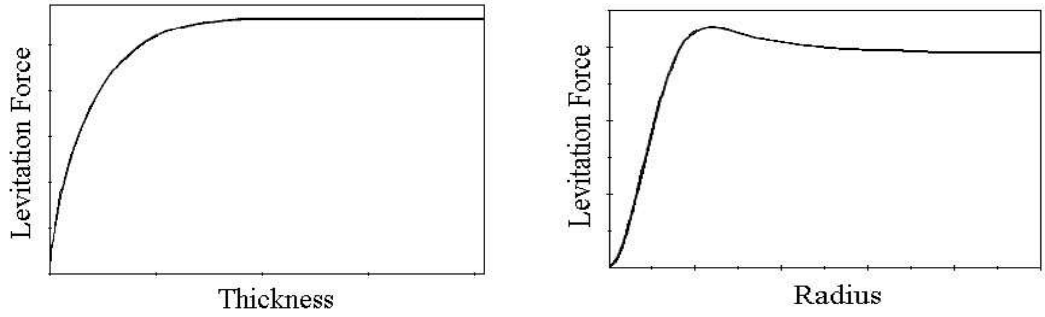

(a) (b)

Figure 2.2: Relation between Levitation Force and (a) HTS Thickness, (b) HTS Radius.

since the test values used by the respective authors differed. However, both clearly showed the same trend in their findings. This important finding leads to one of the major advantages of using HTSs as opposed to conventional magnetic materials; *reduction of size and weight.*

2.2.2 HTS Temperature

The operating temperature of the HTSs is crucial to the proper functioning of the system. Changes in temperature can affect the system in several ways. One way in which shifts in the operating temperature can have adverse effects is by changing the resistance of the HTS. Figure 2.3 illustrates the connection between resistance and temperature.

From figure 2.3 it is evident that a small change in the operating temperature of the HTS (round T_c) causes a large change in resistance. An increase in temperature could lead to an increase in resistance, thereby increasing losses and defeating the advantage of increased efficiency.

Research done by Krabbes et al [22], shows how temperature affects the levitation force between an HTS sample and a magnet (figure 2.4).

Although YBCO becomes superconducting at 90 K, figure 2.4 shows that a peak levitation force is obtained at approximately half that temperature (50 K). Using liquid nitrogen to cool the HTS pellets, although convenient,

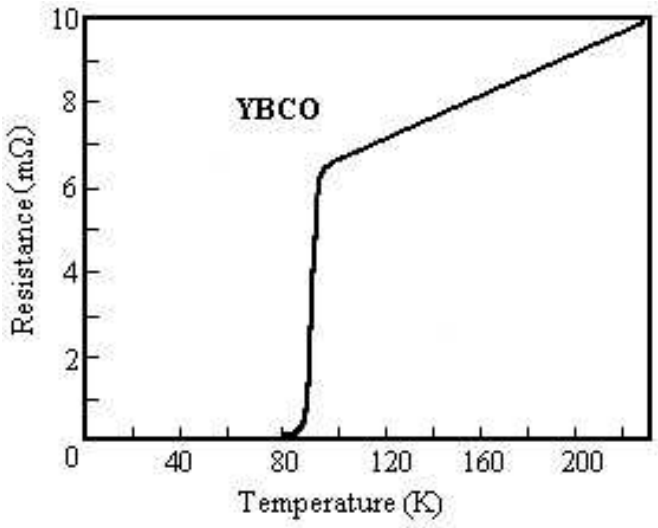

Figure 2.3: Resistance versus Temperature for HTS pellets

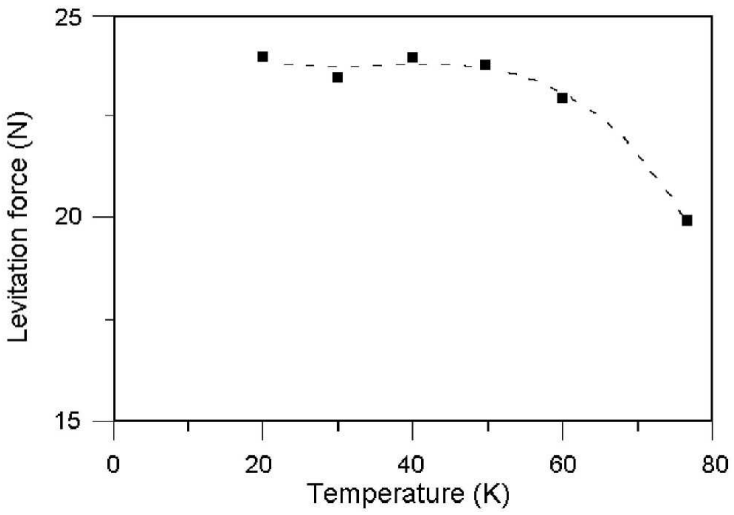

Figure 2.4: Levitation force versus temperature for a YBCO sample

means operating at 77 K and above. Thus if a constant supply of liquid nitrogen is not available the HTS temperature will quickly rise above T_c making accurate measurement difficult. Also operating close to T_c reduces the margin between critical magnetic fields (see Section 2.2.3). Clearly for a superconductor to perform well it should not operate near T_c. As a general "rule of thumb" one should operate at half the value of T_c [23].

2.2.3 "Mixed State"

Superconducting materials become superconductors (zero resistance and zero flux penetration) below temperature T_c and remain so as long as the applied magnetic field does not rise above a critical magnetic field (H_c). Type-II HTSs have a second critical field H_{c2} greater than H_c. When the HTS is in a field (H) where $H_c < H < H_{c2}$, it is known as a "mixed state". In this state, the material still has zero resistance but partial flux penetration is possible. The relationship between H_c and T_c is shown in figure 2.5 [24].

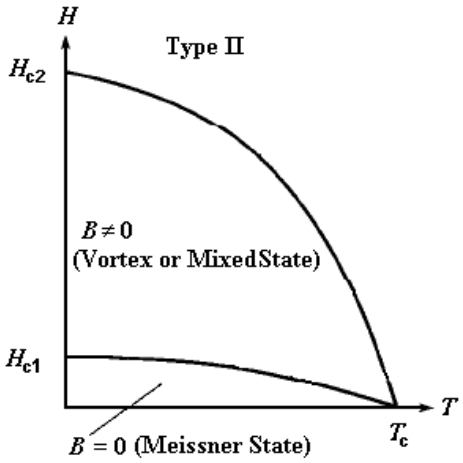

Figure 2.5: The H-T phase space for a type-II superconductor

One advantage of operating the system in this state, is that the HTS does not use up as much energy expelling the flux and thus remains functional in much higher fields than type-I superconductors. Another advantage that comes from operating in the "mixed state" is that of flux pinning [25]. This phenomenon gives rise to hysteretic interaction between the stator and the mover, producing a thrust force in the same manner in which torque is generated in conventional hysteresis motor [26, 27].

2.2.4 "Bean Critical State Model"

In order to appreciate the analytical approach taken in this research in Chapter 3, it is necessary to understand the underlying principles of the "Bean Critical State Model". The best description of this theory is given by Charles Bean himself in his paper on high-field superconductors:

"The basic premise of this theory is that there exists a limiting macroscopic superconducting current density Jc that a hard superconductor can carry; and further, that any electromotive force, however small, will induce this full current to flow locally. On this picture only three states of current flow are possible with a given axis of magnetic field, zero current for those regions that have never felt the magnetic field and full current flow perpendicular to the field axis, the sense depending on the sense of the electromotive force that accompanied the last local change of field [28]."

This description is illustrated, in the plots shown in figure 2.6, for a bulk HTS of radius R.

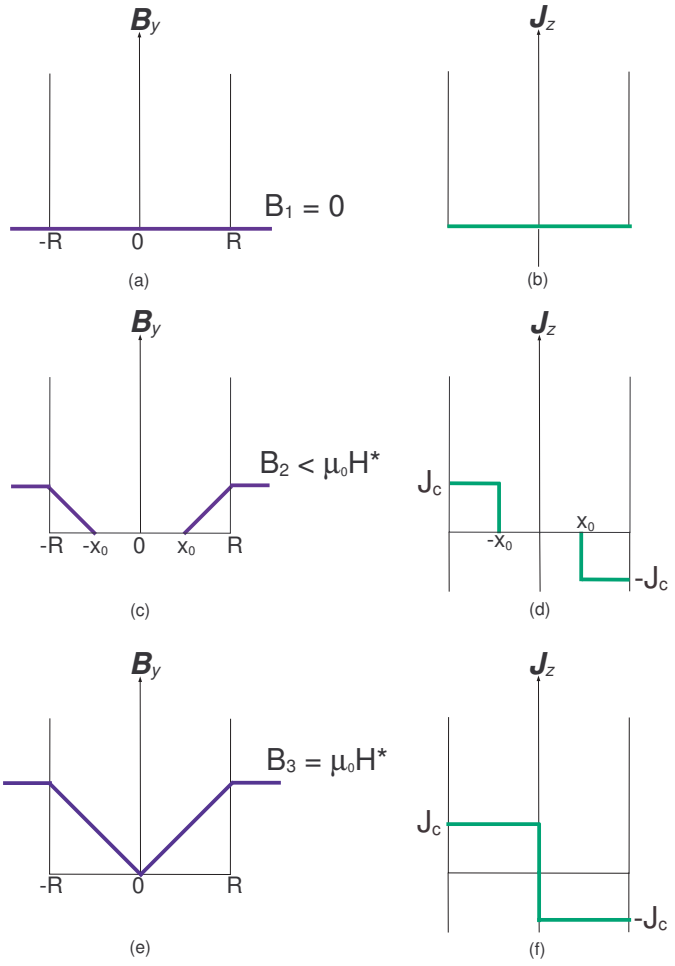

Figure 2.6: Average flux density By and average current density Jz in a bulk superconductor of radius **R** as the field is increased.

Figure 2.6(a) and (b) show that if the applied field is zero then no current flows in the superconductor. In figure 2.6(c) the field is increased and the flux only partially penetrates the superconductor by an amount R-x_0. This causes the critical current Jc to flow in all regions that experienced a flux density $B > 0$ as seen in figure 2.6(d). As $\mathbf{B}$ is increased, flux penetrates further into the slab and the value of x_0 decreases. The value of x_0 is determined from the applied field H_0 as shown in equation 2.1.

$$x_0 = \mathrm{R} - \frac{H_0}{J_c} \tag{2.1}$$

Finally when the field is increased to equal the penetration field H^* (figure 2.6(e)), flux fully penetrates the superconductor and critical current flows at every location in the sample [24]. This is known as the critical state and any further increase in current would lead to quenching of the superconductor, returning it to a normal (non-superconducting) state [25].

Chapter 3

Theoretical Predictions

3.1 Analytical Approach

The analytical model developed in this chapter is loosely based on the approach taken by Barnes, McCulloch and Dew-Hughes [26, 29].

3.1.1 Basic Theory

In order to derive a simple analytical expression for the forces, the problem was broken down into its simplest form consisting of a current carrying conductor and a finite area of HTS as shown in figure 3.1.

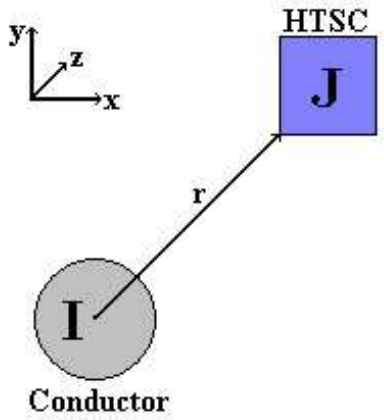

Figure 3.1: Simplified view of relation between HTSC and a conductor

It must be noted that the movement of the HTS in figure 3.1 relative to the conductor is in the x-y plane only. This means that $\mathbf{r}$ varies in x and y directions only.

From the basic motor equation (3.1), a vector equation for the force on a volume element with current density $\mathbf{J}$ can be expressed as shown in (3.2) [30].

$$\mathrm{F} = \mathrm{B\ I\ L} \tag{3.1}$$

$$\mathrm{d}\mathbf{F} = (\mathbf{J} \times \mathbf{B})\,\mathrm{d}V \tag{3.2}$$

where:
F = force on the HTS [N]
B = flux density at the HTS produced by the current in the conductor (x, y direction) [T]
I = current in the conductor (linear motor coils) [A]
L = length of the HTS into the page (z direction) [m]

Since only the forces in the x and y directions are to be considered (thrust and levitation forces), force vector $\mathbf{F}$ can be expressed as a surface integral.

$$\mathbf{F} = \oint \mathbf{J} \times \mathbf{B}\,\mathrm{dA_{HTS}} \tag{3.3}$$

where:
A_{HTS} = cross-sectional area of the HTS [m^2]

The next step is to find an expression for the magnetic field $\mathbf{B}$ in which the HTS is positioned. This field is setup by the conductor and can be found using the Biot-Savart law [31, 32].

$$\mathrm{d}\mathbf{B} = \frac{\mu_o \mathrm{I}}{4\pi} \frac{\mathrm{d}l \times \hat{r}}{\mathrm{r}^2} \tag{3.4}$$

where:
I = current in the conductor [A]
dl = conductor length into the plane [m]
$\hat{\mathbf{r}}$ = unit vector in direction of r [dimensionless]
r = distance between conductor and HTS [m] Note that $\mathrm{r}^2 = r_x^2 + r_y 2$

Solving equation 3.4 for the field B at a distance r from a straight conductor, yields expressions for the magnetic field in both the x and y directions.

$$B_x = -\frac{\mu\,\mathrm{I}\,l_z\,r_y}{2\pi\,|r|^2} \tag{3.5}$$

$$B_y = \frac{\mu \, \mathrm{I} \, l_z \, r_x}{2\pi \, |r|^2} \tag{3.6}$$

Substituting equations 3.6 and 3.5 into equation 3.3 provides a force equation with two components. These are the x and y components of the force or the thrust and levitation forces respectively (see Appendix A: Calculation Details).

$$F_x = \iint_A \frac{-J_z \mu_o I l_z r_x}{2\pi r^2}, \mathrm{d}y\mathrm{d}x \tag{3.7}$$

$$F_y = \iint_A \frac{-J_z \mu_o I l_z r_y}{2\pi r^2}, \mathrm{d}x\mathrm{d}y \tag{3.8}$$

At this point equations have been developed for the forces between a straight wire carrying current I and a finite surface area of the superconductor with current density J flowing in the z direction.

3.1.2 Single Coil and HTS

The analysis is expanded to take into account a superconductor levitating above a current carrying coil. The difference in this case is that there are two conductors carrying current I in opposite directions and there is a current circulating in some outer area of the HTS. This is illustrated in figure 3.2.

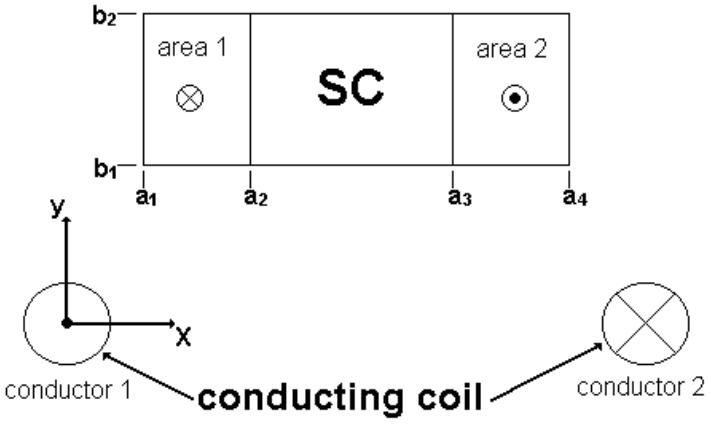

Figure 3.2: Problem layout for single HTS and coil

In order to find the forces between the HTS and the conductor it is necessary

to integrate over the cross-sectional area of the HTS carrying the supercurrent. The integral is first performed for the area carrying the forward current (area 1) and then for the section carrying the return current (area 2). It must be remembered that the sign (+ or −) of J_z depends on the direction of the field that the HTS is exposed to, according to the Bean Model (see Section 2.2.4). Also because the current is circulating in the superconductor, the sign changes depending on the area being integrated. Applying equations 3.7 and 3.8 to this problem gives the forces in the x and y direction (with respect to "conductor 1") as shown in equations 3.9 to 3.12[1].

For Area 1:

$$F_x = \frac{-\mu I l_z J_z}{2\pi} \int_{a_1}^{a_2} \int_{b_1}^{b_2} \frac{r_x}{\left(r_x^2 + r_y^2\right)} \mathrm{d}y\mathrm{d}x \tag{3.9}$$

$$F_y = \frac{-\mu I l_z J_z}{2\pi} \int_{b_1}^{b_2} \int_{a_1}^{a_2} \frac{r_y}{\left(r_x^2 + r_y^2\right)} \mathrm{d}x\mathrm{d}y \tag{3.10}$$

For Area 2:

$$F_x = \frac{-\mu I l_z J_z}{2\pi} \int_{a_3}^{a_4} \int_{b_1}^{b_2} \frac{r_x}{\left(r_x^2 + r_y^2\right)} \mathrm{d}y\mathrm{d}x \tag{3.11}$$

$$F_y = \frac{-\mu I l_z J_z}{2\pi} \int_{b_1}^{b_2} \int_{a_3}^{a_4} \frac{r_y}{\left(r_x^2 + r_y^2\right)} \mathrm{d}x\mathrm{d}y \tag{3.12}$$

This process is then repeated for "conductor 2" by shifting the origin of the reference axes to the centre of "conductor 2" and recalculating the values of a_1 to a_4 (b_1 and b_2 remain the same as there is no change in y-direction) with respect to the new origin. It must also be remembered that the value of I for "conductor 2" is of opposite sign (direction) to that of "conductor 1".

To find the final total forces on the HTS in the x and y direction, the principal of superposition is used. Namely the four x direction forces are added together to give the total thrust force and the four y direction forces are added together to give the total levitation force. Appendix B: MATLAB™ Scripts for Analytical Calculations, contains the listings of the scripts used to perform these calculations and Appendix C: Plots of Analytical Results, contains some sample outputs.

[1]Note that the sign in the equations does not change as the value assigned to J_z can be either positive or negative

3.1.3 3-Phase Supply

When considering a 3-phase sinusoidal supply it is necessary to consider the Critical State Model mentioned in Section 2.2.4. Since the 3-phase coils in the stator will set up a travelling mmf wave, the HTS will be exposed to an alternating applied field. According to the Bean Model the direction of current flow in the HTS is dependent on the sense of the applied field. If one cycle of the field is considered, the direction of rotation of the current in the HTS will alternate as shown in figure 3.3.

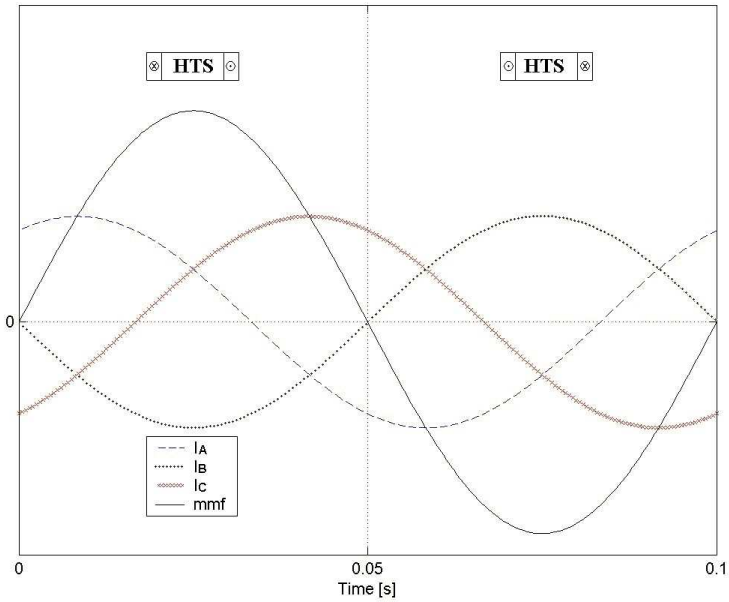

Figure 3.3: HTS current directions for a cycle of the mmf wave (10 Hz)

Figure 3.3 shows that for the first half of the mmf cycle ($t = 0$ s to $t = 0.05$ s) the applied field would be positive and hence the current circulates in a clockwise direction in the HTS. When the negative part of the cycle begins ($t = 0.05$ s to $t = 0.1$ s), the current direction in the HTS reverses. Also shown in figure 3.3 are the current waveforms for each phase.

The same calculation process from section 3.1.2 was used only that this time the force is calculated separately for each of the phase windings in order to take the respective phase currents into account. Also since the value of J_z depends on the *mmf* wave and not the individual current waves, it was decided to

calculate the integration constant for each phase separately.

$$k_A = \frac{-\mu_0 I_A(t)\, l_z J_z}{2\pi} \tag{3.13}$$

$$k_B = \frac{-\mu_0 I_B(t)\, l_z J_z}{2\pi} \tag{3.14}$$

$$k_C = \frac{-\mu_0 I_C(t)\, l_z J_z}{2\pi} \tag{3.15}$$

where:

I(t) = sinusoidal current in respective coil [A]

lz = length into the plane [m]

Jz = critical current density of the HTS [A/m^2]

The direction or sign of J_z will switch with the *mmf* wave. Continuing with the example of a 10 Hz sinusoidal supply, a normalised representation of k_A is as shown in figure 3.4.

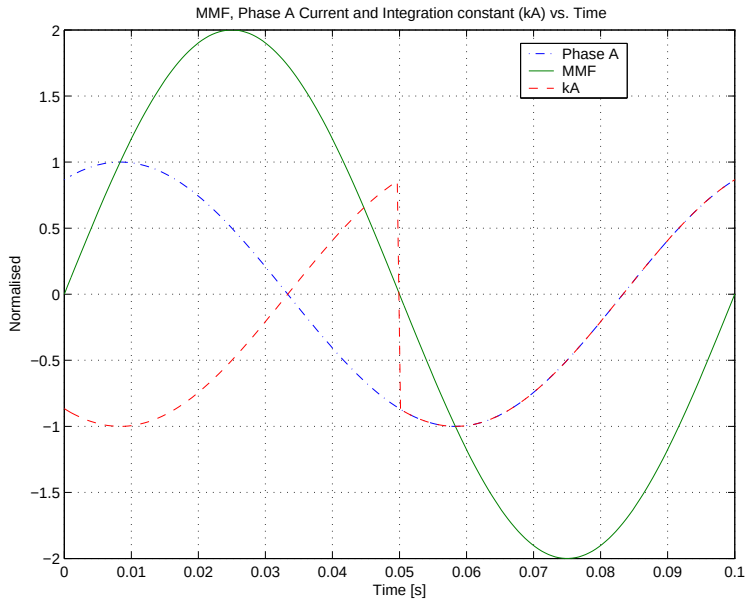

Figure 3.4: Change of integration constant w.r.t the mmf wave ($10Hz$)

For each phase the reference origin is shifted to the center of the appropriate coil in order for the force integral to be calculated. Having calculated the forces on each side of the HTS from both the "in"($\otimes$) and "out"($\odot$) sides of each coil, the summed result is multiplied by the integration constant.

$$Force_A = k_A \times [Fx_{A\ (in\ conductor)\ (left\ area)} + Fx_{A\ (in\ conductor)\ (right\ area)} + Fx_{A\ (out\ conductor)\ (left\ area)} + Fx_{A\ (out\ conductor)\ (right\ area)}] \tag{3.16}$$

$$Force_B = k_B \times [Fx_{B\ (in\ conductor)\ (left\ area)} + Fx_{B\ (in\ conductor)\ (right\ area)}$$

$$+Fx_{B\ (out\ conductor)\ (left\ area)} + Fx_{B\ (out\ conductor)\ (right\ area)}] \quad (3.17)$$

$$Force_C = k_C \times [Fx_{C\ (in\ conductor)\ (left\ area)} + Fx_{C\ (in\ conductor)\ (right\ area)}$$
$$+Fx_{C\ (out\ conductor)\ (left\ area)} + Fx_{C\ (out\ conductor)\ (right\ area)}] \quad (3.18)$$

In the same way it is possible to calculate the forces in the y direction (levitation forces). Total resultant force on the HTS is found by adding the summed forces for each of the three phases together as seen in equation (3.19).

$$TotalForce = Force_A + Force_B + Force_C \quad (3.19)$$

With the method presented so far it is possible to analytically determine the thrust and levitation forces produced on a HTS by a time varying field.

3.1.4 Different HTS Positioning

A further objective of this research is to analyse the forces on a vehicle containing two rows of HTSs and determine the effect of their separation with respect to pole-pitch. This requires the addition of two more sets of force calculations.

$\frac{1}{2}$ Pole-Pitch Separation

The first set of force calculations is for a second HTS placed $\frac{1}{2}$ a pole-pitch away from the first superconductor. Since the same reference axes are used for each phase, the limits of integration in the x direction need to be extended by $\frac{1}{2}$ a pole-pitch. The limits in the y direction need not be changed since both HTSs are at the same height.

Determining the integration constant for the HTS $\frac{1}{2}$ a pole-pitch away requires an inspection of the mmf wave. Figure 3.5 shows that if the first HTS moves along the mmf wave from $t = 0$ s to $t = 0.1$ s the corresponding movement for an HTS $\frac{1}{2}$ a pole-pitch away would be from $t = 0.025$ s to $t = 0.125$ s. From this it can be seen, that whereas HTSs 1 pole-pitch apart only experience one change in mmf direction per cycle, the HTS placed $\frac{1}{2}$ a pole-pitch away will experience 2 changes in mmf direction during the same time frame.

Once again, if we consider the example of the 10 Hz supply, the integration constants for the HTS $\frac{1}{2}$ a pole-pitch away will have two instantaneous "sign"

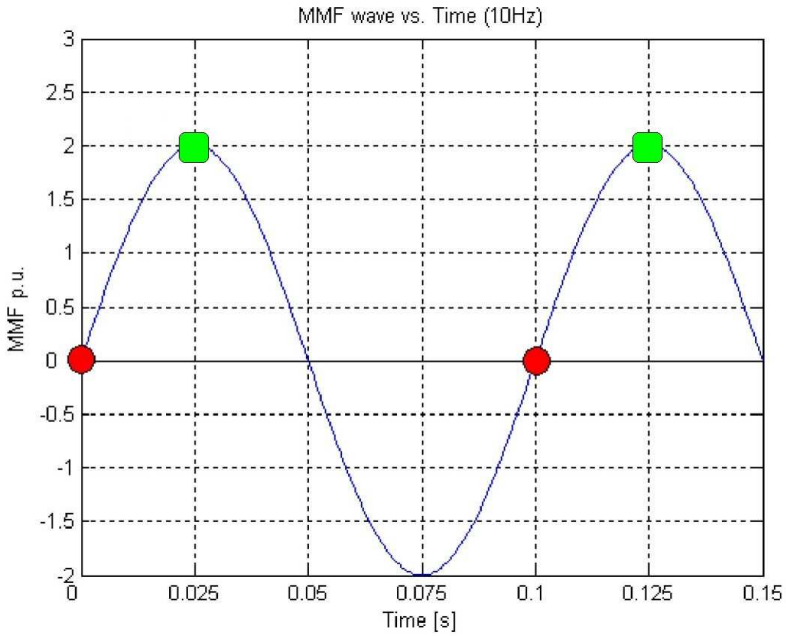

Figure 3.5: Changes in mmf seen by HTSs $\frac{1}{2}$ a pole-pitch apart

changes due to the change in the HTSs current direction. These changes occur at the zero-crossings of the mmf wave seen by the second HTS. This is illustrated in figure 3.6 for the phase-A integration constant k_{Ah}.

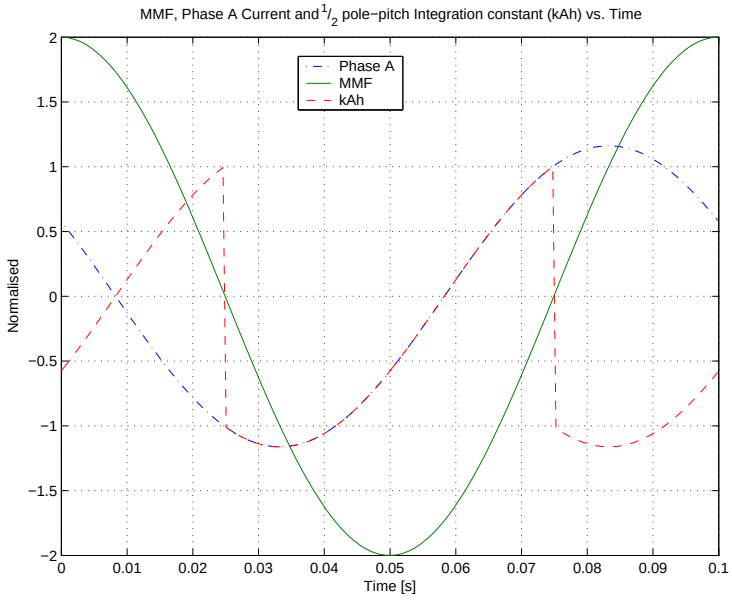

Figure 3.6: Change of integration constant for HTS $\frac{1}{2}$ pole-pitch away ($10Hz$)

Forces are calculated in the same manner as in section 3.1.3. The total force

on a vehicle containing two rows of HTSs separated by $\frac{1}{2}$ a pole-pitch is given by summing the total forces on calculated for each superconductor.

1 **Pole-Pitch Separation**

Another set of calculations is required for a HTS placed exactly 1 pole-pitch away from the original one. Once again the y limits are unchanged whereas the x limits are extended by 1 pole-pitch.

Referring back to figure 3.3 it can be seen that for an HTS 1 pole-pitch away, the mmf will always be in the opposite direction. Thus the current in the HTS will flow in the opposite direction and therefore the value of J_z will be of opposite sign. Considering equations (3.13) to (3.15) and the fact that the mmf value is exactly its negative 1 pole away, the integration constant for this HTS is simply the negative of the first i.e. $-k_A, -k_B$ and $-k_C$.

Having found the forces from each phase on this HTS, the total force on a vehicle containing two rows of HTSs separated by 1 pole-pitch is given by summing the total forces on each of the two superconductors.

3.2 Analytical Results

Before it was possible to calculate the thrust forces for the two topologies, it was necessary to supply the final script (see Appendix B.2) with the relevant operating parameters. The parameters used for the final analytical calculations are shown in table 3.1

The value of critical current was selected from typical values of J_c for melt-textured YBCO superconductors in a field of approximately 1 T [25]. All three phases were given current values which corresponded to the values used in the experiments. Since all the force measurements are taken with the vehicle in a stationary position, it was decided to calculate the forces with the HTS at a predefined starting point. Referring back to figure 3.2, the placement of the HTS with respect to the coil is defined by the starting co-ordinate (a_1, b_1) where a_1 is the levitation height and b_1 is the distance (along the x-axis) of

Table 3.1: Analytical Calculation Parameters

Parameter	**Symbol**	**Value**
HTS Critical Current	J_c	1.00E+07 A/m^2
Supply Current	I_{rms}	10 A
Coil Turns	N	45
HTS area co-ordinate (bottom left)	(x_1, y_1)	(5,1) $[mm]$
HTS area co-ordinate (top right)	(x_2, y_2)	(8,13) $[mm]$
Frequency	f	6 Hz to 15 Hz
HTS width	w	20 mm
Pole pitch	p	57 mm

the HTS from the coil. In the calculations the values (x_1, y_1) were used so as to closely approximate the experiments. The second set of co-ordinates required for the calculation process is (a_2, b_2). The value of b_2 was determined by simply adding the measured height of the HTS pellets to the value used for b_1. In order to select a value for a_2, which would determine the percentage of the HTS used to carry the super-current, the Bean Model was used. Using equation 2.1 it is possible to calculate expected values for flux penetration x_0. In figure 3.2 the value of x_0 is equal to the distance from the centre of the HTS to the point a_2 or a_3. Alternatively the quantity R-x_0 is the same as the distance between a_1 and a_2.

Using the operating parameters of the experimental setup, x_0 was expected to be in the region of 6 mm to 7 mm (see Appendix A.3: HTS Flux Penetration Percentage) and therefore R-x_0 was initially set as 3 mm or 30% of the HTS used and increased towards 40%. The RMS values of the results obtained for a 10 Hz supply current with flux penetration ranging from 30% to 35% for both the 1 and the $\frac{1}{2}$ pole-pitch spacing are shown in table 3.2.

Table 3.2: Calculated RMS thrust forces for 1 and $\frac{1}{2}$ pole-pitch spacing with percentage of flux penetration varying from 30% to 35% [10 Hz]

	Flux Penetration					
	30%	31%	32%	33%	34%	35%
$\frac{1}{2}$ pole-pitch	0.667 N	0.689 N	0.712 N	0.734 N	0.756 N	0.778 N
1 pole-pitch	0.807 N	0.836 N	0.865 N	0.894 N	0.923 N	0.952 N

Only the results for 10 Hz are given because changing the supply frequency proved to have no direct effect on the forces calculated. This can be seen in figure 3.7, which shows the calculated variation of thrust force with both frequency and percentage of flux penetration for the 1 pole-pitch layout.

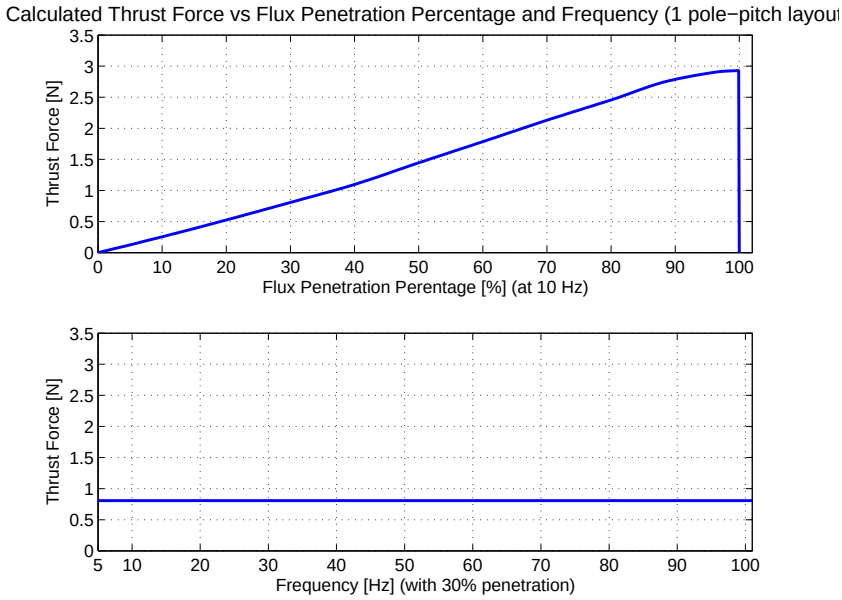

Figure 3.7: Calculated thrust force versus frequency and flux penetration percentage (HTSs 1 pole-pitch apart)

Although the calculations performed were able to determine both thrust and levitation forces, only the thrust forces are shown here as low levitation heights made it unpractical to measure levitation forces experimentally. Appendix C: Plots of Analytical Results, contains individual plots of the thrust forces for various frequencies and amounts of flux penetration.

Chapter 4

Experimental Setup

4.1 Linear Motor Details

In 1999 a prototype Maglev track was built by Vandenbroucke and Zachas [2]. This track was designed in a "U" shape in order to provide thrust, levitation and stability from a single excitation. Since it is the purpose of this research to determine the interaction forces between a travelling magnetic wave and an HTS, and also the direct effects of HTS placement with respect to the pole-pitch, it was decided not to use this "U-shaped" track but rather a flat LM section. This was because it would not be easy to separate the effects due to the HTS placement and those due to the special shaping of the track.

Considering the availability of pre-built linear motor sections it was decided to use an existing track, built for launching a permanent magnet vehicle, as the stator. This track consisted of two LM sections connected in series. Details of the dimensions and windings of this track are given in the forthcoming sections.

4.1.1 Stator Core Dimension

The stator sections used were constructed from the standard laminations produced by the department. These laminations have been designed with semi-closed slots for purposes of increased airgap flux density distribution and less leakage reactance. Dimensions of the stator section are given in table 4.1.

Table 4.1: Dimensions of Linear Motor Primary

Number of slots	30
Slot width	10 mm
Slot depth	42 mm
Tooth width (semiclosed)	9 mm (+7 mm at top end)
Lamination width	0.65 mm
Stator height	82 mm
Stator length	570 mm
Stator width	114 mm
Tolerances	0.5 mm

A diagram showing the dimensions of the stator laminations used is shown in figure 4.1.

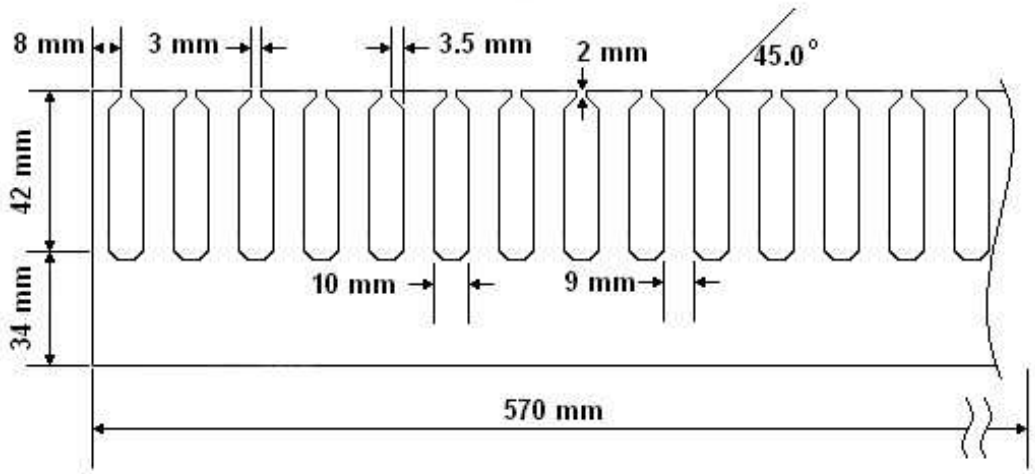

Figure 4.1: Stator Lamination Dimensions

4.1.2 Winding Parameters

Stator winding details for the LM used are shown in table 4.2

Table 4.2: Winding Details

Number of phases	3
Number of poles	10
Number of slots/pole/phase	1
Chording	None
Pole Pitch	57 mm
Number of turns/coil	45
Number of coils/slot	2
Rated Current	16 A
Coil Connection	Parallel

4.2 HTS Maglev Vehicle Details

Two secondary vehicles were constructed from polystyrene, each containing two rows of five bulk HTS pellets. The pellets used are melt-textured YBCO large domain Levitators^{TM} manufactured by Superconductive Components Incorporated (more detailed information about the properties and manufacturing process is available on their website)[18]. In one vehicle the HTSs are separated by 57 mm (1 pole-pitch) and in the other by 85.5 mm ($1\frac{1}{2}$ pole-pitches). The reason for using $1\frac{1}{2}$ and not $\frac{1}{2}$ a pole-pitch is that in building a vehicle with $\frac{1}{2}$ a pole-pitch spacing it proved to be unstable and impractical due to its small length and larger height.

The HTS pellets were fixed into the bottom of the polystyrene vehicle in such a way that each of the five pellets were pressed tightly against each other forming strips 100 mm in length. Holes were drilled in the top of the vehicle directly above each of the pellets in order to contain the liquid nitrogen that would keep the YBCO in its superconducting state. Liquid nitrogen was used because it is freely available at the university and safer to use than liquid helium, even so safety precautions had to be taken when handling the liquid nitrogen (see Appendix D: Liquid Nitrogen Safety Procedures). A diagrammatic representation of the Maglev vehicle layout is shown in figure 4.2. Detailed schematic drawings of both vehicles and the Levitators^{TM} are given in Appendix E: Vehicle Design.

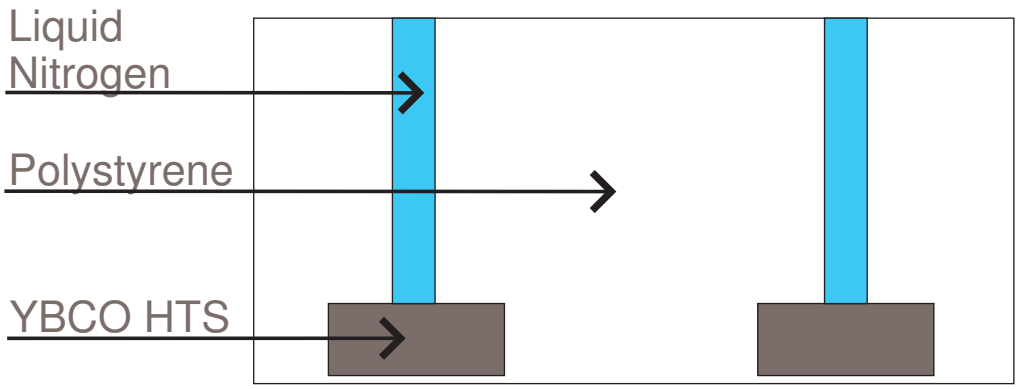

Figure 4.2: Maglev Vehicle Layout

4.3 Experiment Details

The evaluation process consists of a series of force measurements under different excitation conditions. An 3-phase inverter is used to supply the stator sections with a constant current (between 10 A and 11 A) over a range of frequencies (7 Hz to 15 Hz). The Maglev vehicles are "zero-field-cooled" with liquid nitrogen, meaning that the HTSs are brought bellow T_c into their superconducting state outside the presence of a magnetic field. This is done in order to avoid trapping flux within the HTS pellets and creating superconducting permanent magnets which would affect the interaction between HTS and LM. The topic of "field-cooling" will be covered under Recommendations in Section 6.

Since temperature has a direct effect on force (as shown in the Section 2.2.2) and the temperature of liquid nitrogen is only 16°C below the critical temperature of YBCO, it is important to get some measure of the temperature rise. Available temperature probes were not able to measure the extremely low temperatures of HTSs, so it was decided to measure the temperature of the stator windings directly below the HTSs. The high temperature gradient between the coils and the HTSs, and the small airgap between vehicle and motor, causes the liquid nitrogen to boil off faster. For this reason it was decided to not allow the coil temperature to rise above 40°C (about 13°C above ambient of the lab). This way all tests are run with coil temperature at the same level. Thrust force measurements were made using a newton spring balance which was attached to the vehicle via a pulley. The vehicle being tested was pre-cooled and topped up with liquid nitrogen (to keep the vehicle weight

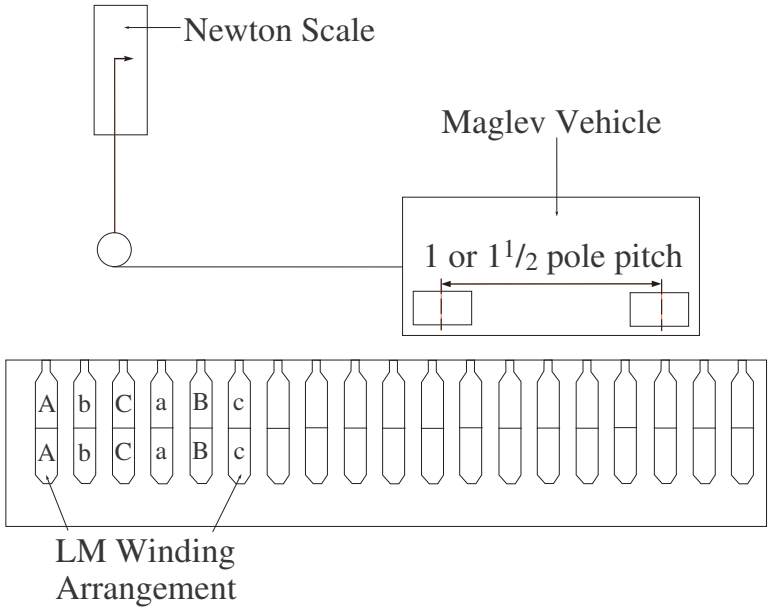

Figure 4.3: Diagram of Experimental Setup

constant for all tests) before being placed at a specific position on the LM. Due to the fact that the flat LM design did not provide any lateral stability, a piece of string (minimal friction) was used on either side of the LM as a guide rail. After a force measurement was taken at the set frequency, the LM was de-energized and allowed to cool down to the starting temperature. Additionally the vehicle was allowed to heat up in order to make sure that no remnant flux remained in the HTSs. This process was followed for each of the test frequencies. The experiments are repeated for both the vehicles with the 1 and the $1\frac{1}{2}$ pole pitch spacing in order to provide a comparison between these two topologies. A diagram of the test setup is shown in figure 4.3.

4.3.1 Experimental Results

Both vehicles had a dry weight of 410 g and weighed 520 g when filled with liquid nitrogen. It should be noted that the resolution of the newton spring balance used is 0.02 N and that all force measurements were taken with coil temperature between 36°C and 40°C.

Table 4.3 shows the results for the vehicle with $1\frac{1}{2}$ pole pitch spacing between HTS rows. The average force for the $1\frac{1}{2}$ pole-pitch spacing is 0.724 N.

Table 4.3: Experimental Results for $1\frac{1}{2}$ pole pitch Spacing

Frequency [Hz]	Line Voltage [V]	Line Curren [A]	Thrust Force [N]
6.7	131	10.3	0.68
7.5	139	10.5	0.7
8.2	145	10.6	0.7
9.2	155	10.7	0.72
10.4	166	10.5	0.7
11.4	176	10.8	0.74
12.4	185	10.6	0.72
13.2	192	10.7	0.76
14.4	203	10.5	0.78
15.4	213	10.4	0.74

Table 4.4 shows the results for the vehicle with 1 pole pitch spacing between HTS rows. The average force for the 1 pole-pitch vehicle is 0.924 N.

Table 4.4: Experimental Results for 1 pole pitch Spacing

Frequency [Hz]	Line Voltage [V]	Line Curren [A]	Thrust Force [N]
6.7	129	10.7	0.88
7.5	135	10.7	0.9
8.2	143	10.7	0.9
9.2	152	10.9	0.9
10.4	163	10.7	0.9
11.4	173	10.8	0.95
12.4	183	10.7	0.95
13.2	190	10.8	0.98
14.4	202	10.7	0.98
15.4	211	10.7	0.9

Chapter 5

Observations

5.1 Discussion of Results

The analytical model predicted that the forces produced on the vehicle with HTSs placed 1 pole-pitch apart would be greater than those of the vehicle with $\frac{1}{2}$ pole-pitch spacing. This much was verified by the experimental measurements with the 1 pole-pitch vehicle having an average force of 0.924 N and the $1\frac{1}{2}$ pole-pitch vehicle having an average force of 0.724 N. The analytical model also revealed that this difference in forces between the two vehicles increases with increasing usage of the HTS. This can be seen clearly in figure 5.1.

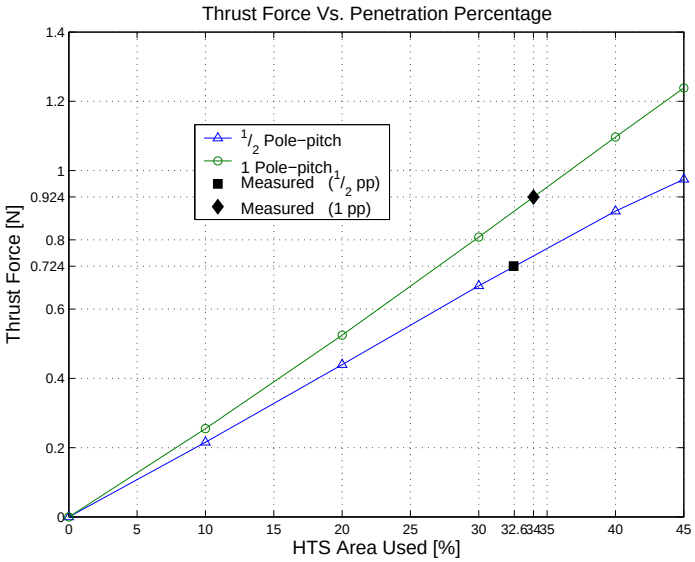

Figure 5.1: Thrust Force versus Percentage of HTS Used for 1 and $\frac{1}{2}$ pole-pitch Layouts

Furthermore if a closer look is taken at the percentage of the HTS being used, the analytical model suggests that the amount of HTS being used to carry current should lie in the region of 34% for both experiments. The expected amount of flux penetration for the experiments (as calculated in Appendix A.3) corresponds to 34.1% of the HTS being used. From figure 5.1 it can be seen that the average force measured with the 1 pole-pitch vehicle corresponds to 34%, whereas the average force measured with the $1\frac{1}{2}$ pole-pitch vehicle corresponds to 32.6% of the HTS area used. The difference in predicted and measured thrust forces is shown in table 5.1.

Table 5.1: Comparison of measured and predicted thrust forces

	$\frac{1}{2}$ pole-pitch	1 pole-pitch
Predicted	0.756 N	0.923 N
Measured	0.724 N	0.924 N
Error	0.032 N	0.001 N

Considering that the resolution of the force measurement equipment was 0.02 N, the bigger error in the $\frac{1}{2}$ pole-pitch prediction is reasonable. This shows good correlation between measured and predicted results. Another possible cause of the discrepancy in the predicted results for the $\frac{1}{2}$ pole-pitch topology is due to an inherent error caused by the **arctan** function in the force calculations. This error is discussed further in Section 5.2.

5.2 Problems with Analytical Model

The integral equation used to calculate the forces in the analytical model is considered in its general form as in equation 5.1.

$$F_x = \int_{x_1}^{x_2} \int_{y_1}^{y_2} \frac{x}{(x^2 + y^2)} \mathrm{d}y\mathrm{d}x \tag{5.1}$$

An analysis of the integral solution with respect to the starting position of the HTS (x_1) revealed that the solution became invalid for very small values of x_1. This is best illustrated in the plot of the general solution to equation 5.1 versus the starting point x_1 seen in figure 5.2 (a).

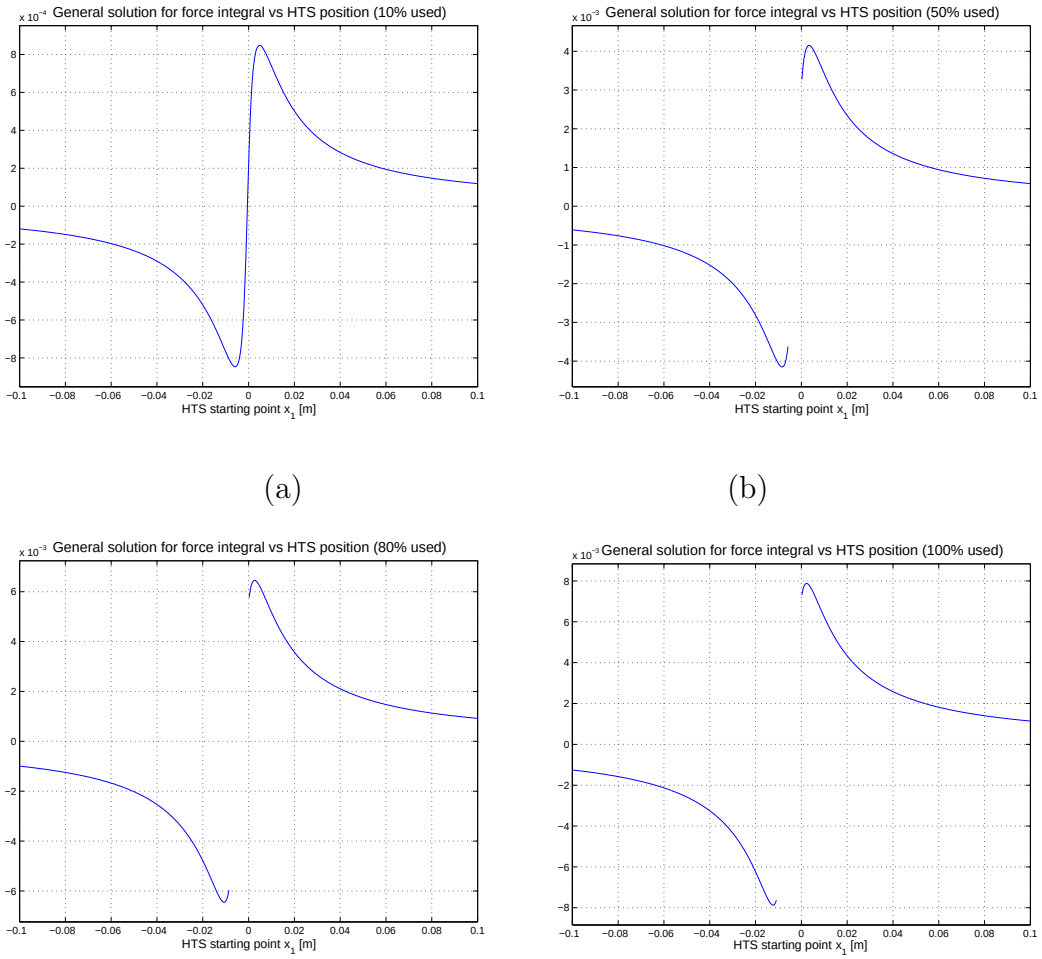

Figure 5.2: General Solution to Force Equation versus Starting Co-ordinate: (a) 10% of HTS Used, (b) 50% of HTS Used, (c) 80% of HTS Used, and (d) 100% of HTS Used.

Examining figure 5.2 (a) reveals that values of x_1 that lie to the left of the peak in the first quadrant would yield invalid results. In this region an increase in the distance between current source and magnetic field (x_1) results in an increase in force. The problem is increased further by the fact that the space between conductors is less than the width of the HTS, meaning that when one end of the HTS is a valid distance away from the first conductor the other end may be in an error region with respect to the second conductor. Also the fact that two HTSs were being considered in the calculations made it more difficult to stay out of the error region. This was particularly evident in the case of the $\frac{1}{2}$ pole-pitch spacing as can be seen from the results in Appendix C.2.

Furthermore it was discovered that increasing the percentage of HTS being used (integration area) also increases the range of unacceptable values for x_1. This can be seen in figures 5.2 (b) to 5.2 (d). The distance between the peaks of the graph increases from 0.01 m (when 10% of the HTS is used) to 0.014 m (when 100% of the HTS is used). This translates to a 4 mm band of unacceptable values for the starting coordinate of the HTS, which is significant when considering the gap between coils is only 19 mm.

Chapter 6

Conclusions and Recommendations

6.1 Concluding Remarks

The objective of this research was to provide a better understanding of the forces experienced by bulk high-temperature superconductors (HTSs) levitating above linear motors (LMs). This was achieved by developing an analytical approach for calculating the forces between bulk HTSs and 3-phase conducting coils. Also a prototype MagLev system was built in order to meet the secondary objective of analysing the effect of HTS positioning with respect to LM pole-pitch.

In order to better understand the interaction between HTSs and the travelling magnetic wave produced by the LM coils,the analytical model was developed by firstly considering the simplest form of the problem (one HTS and one conductor) using basic magnetic principles ($\mathbf{J} \times \mathbf{B}$). This was then adapted to take the MMF wave produced by a 3-phase system into account and calculate the forces produced on different sets of HTSs. The model predicted that HTSs spaced 1 pole-pitch apart would experience a greater resultant force from a LM than HTSs spaced only $\frac{1}{2}$ a pole-pitch apart.

Analytical predictions were verified on prototype MagLev system. Measurements performed on a vehicle containing HTSs spaced 1 pole-pitch apart,

showed forces to be in the region of 27% greater than on the vehichle $1\frac{1}{2}$ pole-pitch spacing. From the operating parameters of the protoype it was deterimined that 34% of the HTSs was being used. For this amount of HTS usage the anlytical model predicted the forces with less 1% error in the 1 pole-pitch case and less than 5% error $1\frac{1}{2}$ pole-pitch in the case. This error is attributed to numerical limitations of the analytical model and the resolution of the measurement equipment.

Overall this research provided insight into the basic principles governing the interaction between bulk high-temperature superconductors and travelling magnetic waves. It must be remembered that the field of HTSs is still in its initial phases and that with the advances being made in HTS production, it will not be long before applications making use of the low-weight, low-loss, levitated and frictionless advantages of these materials. Thus the author believes that there is merit in continuing in this line of research by improving the modelling technique and performing further experiments such as those suggested in the following section.

6.2 Future Work

A recommended extension to this research is to investigate the use of field-cooled HTSs in the vehicle. This will allow for a comparison of zero-field cooled and field cooled systems. Furthermore it will be possible to develop a more accurate analytical model since the magnetic field in the HTS can be directly measured and thus treated as a strong permanent magnet.

There are various methods for magnetising (field-cooling) HTSs. In particular Tsukamoto et al. [33] provide a method of magnetising an array of HTSs, where each HTS has alternate polarity, in a single process. Alternatively, flux trapping through pulsed magnetization with temperature control [34] or controlling of the pulse rise time [35]. The benefits of pulsed magnetization are that a strong external magnetic field is not required for the magnetization process. However, it has been shown that higher trapped fields have been achieved through steady-state methods [35].

Ultimately it would be desirable to harness the benefits of both field-cooled

and zero-field-cooled HTSs. This entails investigating a hybrid system such as the one presented by Muramatsu et al. [36] where zero-field-cooled HTSs are placed above the LM for thrust and field-cooled HTSs are placed above a PM guide way for stability. This type of system will allow for higher thrust forces [37] and increased levitation height and stability [38].

References

[1] A R Jha. *Superconducting Technology*. John Wiley and Sons, New York, 1998.

[2] K Vandenbroucke and A Zachas. Design and Evaluation of a High Temperature Superconducting Maglev System. Technical report, University of the Witwatersrand, Johannesburg, 1999.

[3] Gautrain Rapid Rail Link. `http://www.gautrain.co.za/source/contents/documents/InceptionReport-15June2000.pdf`. Last accessed 10 February 2004.

[4] F C Moon. *Superconducting Levitation: Applications to Bearings and Magnetic Transportation*. John Wiley and Sons, 1994.

[5] T P Sheahen. *Introduction to High-Temperature Superconductivity*. Plenum Press, 1994.

[6] R G Rhodes and B E Mulhall. *Magnetic Levitation for Rail Transport*. Claredon Press, Oxford, 1981.

[7] Y K Kim, M Katsurai, and H A Fujita. A Superconducting Actuator Using the Meissner Effect. In *Sensors and Actuators*, volume 20, page 33, 1989.

[8] T Azukizawa, M M Morishita, N Kasahara, et al. Characteristics of Magnets Suspensions System Using High Tc Superconductors. In *Proceedings of the International Symposium on Non-Linear Phenomena in Electromagnetic Fields*. ISEM-Nagoya, January 1992.

[9] D Wolfshtein, T E Seidel, D W Johnson Jr., et al. A Superconducting Magnetic Levitation Device for the Transport of Light Payloads. In *J. Supercond.*, volume 2, page 211, 1989.

[10] J R Hull and A Cansiz. Vertical and Lateral Forces Between a Permanent Magnet and a High-Temperature Superconductor. In *J. Appl. Phys.*, volume 86, pages 6396–6404, 1999.

[11] L K Kovalev, K V Ilushin, S M A Koneev, et al. Hysteresis and Reluctance Electric Machines with Bulk HTS Rotor Elements. In *IEEE Trans. Appl. Supercond.*, volume 9, pages 1261–1264, June 1999.

[12] B Oswald, M Krone, M Söll, et al. Superconducting Reluctance Motors with YBCO Bulk Material. In *IEEE Trans. Appl. Supercond.*, volume 9, pages 1201–1204, June 1999.

[13] G J Barnes, M D McCulloch, and D Dew-Hughes. Torque from Hysteresis Machines with Type-II Superconducting Segmented Rotors. In *Physica C*, 331, pages 133–140. 2000.

[14] T Habisreuther, T Straßer, W Gawalek, et al. Magnetic Processes in Hysteresis Motors Equipped with Melt-Textured YBCO. In *IEEE Trans. Appl. Supercond.*, volume 7, pages 900–903, June 1997.

[15] M Zeisberger, T Habisreuther, D Litzkendorf, et al. Optimization of Levitation Forces. *IEEE Trans. Appl. Supercond.*, 11(1):1741–1744, March 2001.

[16] I-G Chen, J-C Hsu, and M-K Wu. Calculation of Magnetic Levitation/Suspension Forces of Single Grained Y-Ba-Cu-O Superconductors. *IEEE Trans. Appl. Supercond.*, 11(1):1745–1748, March 2001.

[17] I G Chen, G Jamn, J C Hsu, and M K Wu. Materials Characteristics of Single-Grained Y-Ba-Cu-O Superconductor. In *J. Appl. Phys.*, volume 81, pages 4947–4979, 1997.

[18] SCI Engineered Materials: Superconductive Components Inc. (Suppliers of the Melt Textured YBCO Levitators^{TM}). `http://www.superconductivecomp.com/products/levitators/`. Last accessed 10 February 2004.

[19] Oak Ridge National Laboratory. (A Teacher's Guide to Superconductivity for High School Students). `http://www.ornl.gov/reports/m/ornlm3063r1/contents.html`. Last Accessed 10 February 2004.

[20] J Lugo and V Sosa. Levitation Force Between a Small Magnet and a Superconducting Sample of Finite Size in the Meissner State. In *Physica C*, volume 324, pages 9–14, 1999.

[21] S Sagar, K Lahiri, D Shi, and J Z Yang. Effect of Sample Geometry on Levitation Force in Seeded-Melt-Grown Single-Domain $YBa_2Cu_3O_x$. In *IEEE Trans. Appl. Supercond.*, volume 7, pages 1929–1932, June 1997.

[22] G Krabbes, P Schätzle, W Bieger, et al. Thermodynamically Controlled Melt Processing to Improve Bulk Materials. In *IEEE Trans. Appl. Supercond.*, volume 7, pages 1735–1738, June 1997.

[23] K Fitzgerald. Superconductivity: Fact vs. Fancy. In *IEEE Spectrum*, volume 25, pages 33–41, May 1988.

[24] Terry P Orlando and Kevin A Delin. *Foundations of Applied Superconductivity*. Addison-Wesley Publishing Company, New York, 1991.

[25] James D Doss. *Engineer's Guide to High-Temperature Superconductivity*. John Wiley and Sons, New York, 1989.

[26] G J Barnes, M D McCulloch, and D Dew-Hughes. Finite Difference Modelling of Bulk High Temperature Superconducting Cylindrical Hysteresis Machines. In *Supercond. Sci. Technol.*, volume 13, pages 229–236, 2000.

[27] R J Cruise, K Vandenbroucke, C F Landy, et al. Design and Evaluation of a High Temperature Superconducting Maglev System. In *Physica C: Superconductivity*, volume 341-348, pages 2627–2628, 2000.

[28] C P Bean. Magnetization of High-Field Superconductors. In *Rev. Mod. Phys.*, volume 36, pages 31–39, 1964.

[29] G J Barnes, M D McCulloch, and D Dew-Hughes. Computer Modelling of Type II Superconductors in Applications. In *Supercond. Sci. Technol. 12*, pages 518–522, 1999.

[30] John D Kraus. *Electromagnetics*. McGraw-Hill. Inc., fourth edition, 1991.

[31] Douglas C Giancoli. *Physics for Scientists and Engineers*. Prentice Hall, second edition, 1988.

[32] V Pyati. Simplified Biot-Savart Law for Planar Circuits. In *IEEE Trans. on Educ.*, volume E-29, pages 32–33, 1986.

[33] O Tsukamoto, J Ogawa, M Iwamoto, et al. Magnetization of HTS Bulk Array with Alternate Polarities for Linear Superconducting Actuator. In *Physica C*, 354, pages 18–22. 2001.

[34] H Kamijo and H Fujimoto. Repeated Pulsed-Field Magnetization with Temperature Control in a High-Tc Bulk Superconductor. *IEEE Trans. Appl. Supercond.*, 11(1):1816–1819, March 2001.

[35] T Ishigohka, H Ichikawa, A Ninomiya, et al. Flux Trapping Characteristics of YBCO Bulks Using Pulse Magnetization. *IEEE Trans. Appl. Supercond.*, 11(1):1980–1983, March 2001.

[36] R Muramatsu, S Sadakata, M Tsuda, and A Ishiyama. Trial Production and Experiments of Linear Actuator with Bulk Secondary. *IEEE Trans. Appl. Supercond.*, 11(1):1976–1979, March 2001.

[37] K B Ma, Y Postrekhin, H Ye, and W K Chu. Magnetic Interaction Force Between High-Tc Superconductor-Ring and Magnet. *IEEE Trans. Appl. Supercond.*, 11(1):1665–1668, March 2001.

[38] Y Sanagawa, H Ueda, M Tsuda, et al. Characteristics of Lift and Restoring Force in HTS Bulk: Application to Two-Dimensional Maglev Transporter. *IEEE Trans. Appl. Supercond.*, 11(1):1797–1800, March 2001.

Appendices

Appendix A

Calculation Details

A.1 Biot-Savart Law

$$\mathrm{dB} = \frac{\mu}{4\pi} \frac{\mathrm{I}\,\mathrm{d}\mathbf{l}\,\sin\theta}{\mathrm{r}^2} \tag{A.1}$$

or in vector notation,

$$\mathrm{dB} = \frac{\mu\,\mathrm{I}}{4\pi} \frac{\mathrm{d}\mathbf{l} \times \mathbf{r}}{|\mathbf{r}|^2} \tag{A.2}$$

Pyati [20] shows that for a planar circuit, the field **B** at a distance r from a straight conductor is given by:

$$\begin{aligned} |\mathbf{B}| &= \frac{\mu\,\mathrm{I}}{4\pi} \int_{-\pi/2}^{+\pi/2} \frac{\mathrm{d}\theta}{\mathbf{r}} \\ &= \frac{\mu\,\mathrm{I}}{4\pi r} \int_{-\pi/2}^{+\pi/2} \cos\theta\,\mathrm{d}\theta \\ &= \frac{\mu\,\mathrm{I}}{2\pi r} \end{aligned} \tag{A.3}$$

Since for this research it is necessary to determine both the x and y components of the magnetic field **B**, the cross product in equation A.2 is solved to yield the following:

$$\begin{aligned} \mathrm{d}\mathbf{l} \times \mathbf{r} &= \det \begin{vmatrix} i & j & k \\ 0 & 0 & l_z \\ r_x & r_y & 0 \end{vmatrix} \\ &= \left[-i\,(l_z \cdot r_y) + j\,(l_z \cdot r_x)\right] \end{aligned} \tag{A.4}$$

which leads to the expressions for B_{x} and B_{y}

$$B_x = -\frac{\mu \, \mathrm{I} \, \mathrm{l_z} \, \mathrm{r_y}}{2\pi \left|r\right|^2} \tag{A.5}$$

$$B_y = \frac{\mu \, \mathrm{I} \, \mathrm{l_z} \, \mathrm{r_x}}{2\pi \left|r\right|^2} \tag{A.6}$$

where:

$$\left|r\right|^2 = \left(\mathrm{r_x^2} + \mathrm{r_y^2}\right)$$

This solution can be checked by simply summing the squares of equations A.5 and A.6 to obtain the square of equation A.3 as shown below:

$$\begin{aligned} \left|\mathbf{B}\right|^2 &= {B_x}^2 + {B_y}^2 \\ &= \frac{\mu^2 \, \mathrm{I}^2 \left({\mathrm{r_y}}^2 + {\mathrm{r_x}}^2\right)}{2\pi r^2} \\ &= \frac{\left(\mu \, \mathrm{I} \, \mathrm{r}\right)^2}{\left(2\pi r^2\right)^2} \\ &= \frac{\mu \, \mathrm{I}}{2\pi r} \end{aligned} \tag{A.7}$$

A.2 Force Integral

The thrust and levitation forces are determined by integrating the cross product of the current density in the HTS ($\mathbf{J}$) and the magnetic field ($\mathbf{B}$) over a finite surface area.

$$\mathbf{F} = \oint \mathbf{J} \times \mathbf{B} \, \mathrm{dA}_{HTS} \tag{A.8}$$

The result of $\mathbf{J} \times \mathbf{B}$ is found as follows:

$$\begin{aligned} \mathbf{J} \times \mathbf{B} &= \det \begin{vmatrix} \mathrm{i} & \mathbf{j} & \mathrm{k} \\ 0 & 0 & \mathbf{J}_{\mathrm{z}} \\ \mathbf{B}_{\mathrm{x}} & \mathbf{B}_{\mathrm{y}} & 0 \end{vmatrix} \\ &= \mathrm{i} \ \left(-\mathbf{J}_{\mathrm{z}} \cdot \mathbf{B}_{\mathrm{y}}\right) + \mathrm{j} \ \left(\mathbf{J}_{\mathrm{z}} \cdot \mathbf{B}_{\mathrm{x}}\right) \end{aligned} \tag{A.9}$$

Substituting the solution to equation A.9 into equation A.8 gives the integral equations for the force in the x and y directions

$$\mathrm{F}_x = \frac{-\mu\ \mathrm{I}}{2\pi} \int_{\mathrm{y}_1}^{\mathrm{y}_2} \int_{\mathrm{x}_1}^{\mathrm{x}_2} \frac{\mathrm{J_z\ r_x}}{\left(\mathrm{r_x^2 + r_y^2}\right)} \,\mathrm{d}y\,\mathrm{d}x \tag{A.10}$$

$$\mathrm{F}_y = \frac{-\mu\ \mathrm{I}}{2\pi} \int_{\mathrm{x}_1}^{\mathrm{x}_2} \int_{\mathrm{y}_1}^{\mathrm{y}_2} \frac{\mathrm{J_z\ r_y}}{\left(\mathrm{r_x^2 + r_y^2}\right)} \,\mathrm{d}x\,\mathrm{d}y \tag{A.11}$$

A general solution to the the double integral of $\frac{x^2}{x^2+y^2}$ is:

$$\mathrm{F}_x = -x \arctan(\frac{y}{x}) + y \ln(\frac{y}{x}) - 1/2\, y \ln(1 + \frac{y^2}{x^2}) \tag{A.12}$$

A.3 HTS Flux Penetration Percentage

The percentage of the HTS that will carries current is determined by the distance that the flux penetrates into the HTS.

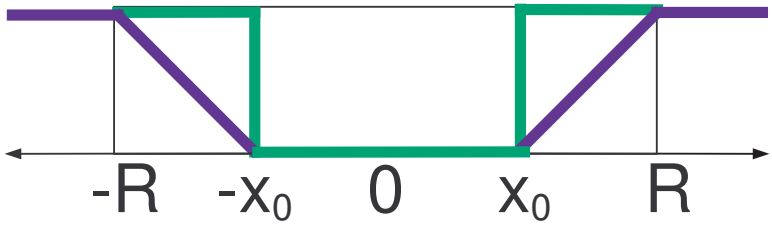

Figure A.1 Flux Penetration and Current Density in HTS

In figure A.1 the blue line represents the magnetic field **B** penetrating the HTS (of radius R) and decreasing linearly to zero and the green line shows that the current flows in the HTS only where a magnetic field exists. SInce $\mathrm{x_0}$ is the distance from the centre of the HTS to the point where flux no longer penetrates i.e. where $\mathbf{B} = 0$, to find the percentage of the HTS used to carry current $\mathrm{R} - \mathrm{x_0}$ is calculated as shown:

$$\mathrm{R} - \mathrm{x_0} = \frac{\mathrm{H_0}}{J_c} \tag{A.13}$$

The value of J_c is constant and the value of $\mathrm{H_0}$ is estimated by first calculating the flux density $\mathrm{B_0}$ in the air-gap above the LM. In order to calculate $\mathrm{B_0}$, the flux per pole (ϕ) is found using equation A.14 and divided by the area of a pole (A) as in equation A.15. $\mathrm{H_0}$ is then determined by dividing this result by the permeability of free space (μ_0) and proportioning it by the ratio of HTS area (A_{HTS}) to pole area as in equation A.16. The constants used are given in table A.1.

Table A.1 Constants used for calculating x_0

A_{HTS} (mm^2)	4000
A (mm^2)	6498
Ratio	0.616
μ_0 (H/m)	$4\pi \times 10^{-7}$
J_c (A/m^2)	10^7
R (mm)	10

$$\phi = \frac{V}{4.44\, f\, N\, k_w} \tag{A.14}$$

$$B_0 = \frac{\phi}{A} \tag{A.15}$$

$$H_0 = \frac{B_0}{\mu_0} \times \frac{A_{HTS}}{A} \tag{A.16}$$

In order to get an estimate of the value of x_0, the operating parameters given in table A.2 were used for solving equations A.13 to A.16.

Table A.2 Operating Parameters for Experiments

f (Hz)	V_l (V)	V_p (V)	I (A)
6.7	131	75.63	10.5
7.5	139	80.25	10.5
8.2	145	83.72	10.6
9.2	155	89.49	10.7
10.4	166	95.84	10.5
11.4	176	101.61	10.8
12.4	185	106.81	10.6
13.2	192	110.85	10.7
14.4	203	117.20	10.5
15.4	213	122.98	10.4
Average	170.5	98.44	10.58

The calculated values of flux density, applied field, x_0 and the resulting percentage of HTS used are shown in table A.3.

From this it can be seen that the expected amount of HTS area being used to transport current is in the region of 34% for the experimental setup.

Table A.3 HTS Flux Penetration (R-x_0)

ϕ (mWb)	B_0 (T)	H_0 ($A/_m$)	x_0(mm)	Percentage of HTS used (%)
0.565	0.087	69191	5.74	42.6
0.536	0.082	65585	5.96	40.4
0.511	0.079	62576	6.15	38.5
0.487	0.075	59620	6.33	36.7
0.461	0.071	56484	6.52	34.8
0.446	0.069	54633	6.64	33.6
0.431	0.066	52796	6.75	32.5
0.42	0.065	51473	6.83	31.7
0.407	0.063	49887	6.93	30.7
0.4	0.062	48945	6.99	30.1
0.453	0.070	55456	6.48	34.1

Appendix B

MATLAB™ Scripts for Analytical Calculations

It should be noted that in order for the MATLAB™ scripts presented in this appendix to function correctly, the *Symbolic Toolbox* is required.

B.1 Single Coil and Superconductor

Firstly a MATLAB™ script was written to perform the basic force calculations (between a single HTS pellet and a single coil carrying a constant current). This script polled the user for relevant information such as HTS dimensions, coil width and current values.

```
%--------------------------------------------------------------------
%--------------------------------------------------------------------
%                            ##  BEGIN  ##
%--------------------------------------------------------------------

echo on
clc
% This program calculates the thrust and levitation forces
% between a current carrying coil and a high-temperature
% superconductor (HTS) pellet.
echo off
x=sym('x');
y=sym('y');
Fx = sym('Fx');
```

```
Fy = sym('Fy');
u=pi*4*1e-7;
d1 = input('Please enter distance between ends of coil (in mm) :');
y1 = input('Please enter height of HTS above coil (in mm) :');
h = input('Please enter height of HTS pellet (in mm) :');
w = input('Please enter width of HTS pellet (in mm) :');
a = input('Please enter percentage of HTS to carry Jc (0-100) :');
x1 = input('Please enter starting point on x-axis (in mm) :');

%-----------------------------------------------------------------------
%initial co-ordinates for the HTS pellet
y2=y1+h;
x2=x1+((w/2)*(a/100));
x3=x2+(w*(100-a)/100);
x4=x3+((w/2)*(a/100));
echo on
clc

%-----------------------------------------------------------------------
%We now need to know the following parameters: (Jc and I)
echo off
Jc = input('Enter the HTS current density [A/m^2] (eg 1e7):');
i = input('Enter the current in the coil [A]:');
N = input('Enter the number of turns per coil:');
I=i*N;
echo on
clc

%-----------------------------------------------------------------------
%Calulating the thrust (Fx) and levitation (Fy) forces for the HTS
echo off

%First conductor (I +ve) Left and Right side of HTS
F1yl = int(int(y/(x^2+y^2),x,x1/1000,x2/1000),y,y1/1000,y2/1000);
F1xl = int(int(x/(x^2+y^2),y,y1/1000,y2/1000),x,x1/1000,x2/1000);
F1yr = -int(int(y/(x^2+y^2),x,x3/1000,x4/1000),y,y1/1000,y2/1000);
F1xr = -int(int(x/(x^2+y^2),y,y1/1000,y2/1000),x,x3/1000,x4/1000);

%Second conductor (I -ve) Left and Right side of HTS
```

```
F2yl = -int(int(y/(x^2+y^2),x,(-d1+x1)/1000,(-d1+x2)/1000),y,...
 ...y1/1000,y2/1000);
F2xl = -int(int(x/(x^2+y^2),y,y1/1000,y2/1000),x,...
 ...(-d1+x1)/1000,(-d1+x2)/1000);
F2yr = int(int(y/(x^2+y^2),x,(-d1+x3)/1000,(-d1+x4)/1000),y,...
 ...y1/1000,y2/1000);
F2xr = int(int(x/(x^2+y^2),y,y1/1000,y2/1000),x,...
 ...(-d1+x3)/1000,(-d1+x4)/1000);

%Sum up the x and y forces
ForceX = (-u*Jc*I/(2*pi))*eval(F1xl+F1xr+F2xl+F2xr);
ForceY = (-u*Jc*I/(2*pi))*eval(F1yl+F1yr+F2yl+F2yr);
echo on
clc
ForceX
ForceY
end
%------------------------------------------------------------------------
%                              ##  END  ##
%------------------------------------------------------------------------
%------------------------------------------------------------------------
```

This script was then converted into a MATLAB™ function. The data that the previous script polled the user for, is now passed to the function via input variables.

```
function [ForceX,ForceY] = calcforce(a1,b1,a2,b2,w,i,p)
%--------------------------------------------------------------------
% [Fx,Fy] = CALCFORCE is a function that calculates the thrust and
% levitation forces between a current carrying coil and a high-
% temparature superconductor (HTS) pellet.
%
% [A,B] = CALCFORCE(x1,y1,x2,y2,w,I,p) where (x1,y1) and (x2,y2) are
% the bottom left and top right co-ordinates of the superconductor
% area carrying current Jc (origin at centre of left conductor), w is
% the HTS pellet width, I is the bulk coil current (current x turns)
% and p is the distance between coil sides (coil pitch).
% [all lengths in mm]
%
% This function Returns:
%                       A = thrust force [N]
%                       B = levitation force [N]
%
%                                  (x2,y2)
%                           .-------o---------.-------.
%                           |  +Jc  |         |  -Jc  |
%                           |       |         |       |
%              y^     (x1,y1)o-------'---------'-------'
%               |            |<--------- w ----------->|
%               |
%             __|__                                        ____
%            |  |  |                                     |    |
%            |  *----------->x                           | -I |
%            |  +I |                                     |    |
%             -----                                      ____
%               |<------------------ p --------------------->|
%
%

%--------------------------------------------------------------------
%                           ##  BEGIN  ##
%--------------------------------------------------------------------
```

```
% constants
x=sym('x');
y=sym('y');
Fx = sym('Fx');
Fy = sym('Fy');

%--------------------------------------------------------------------
%initial co-ordinates for the HTS pellet
d1 = p;
y1 = b1;
y2 = b2;
x1 = a1;
x2 = a2;
x4 = x1+w;
x3 = x4-(x2-x1);

%--------------------------------------------------------------------
%We now need to know the following parameters:
u=pi*4*1e-7;
Jc=1e7;
I = i;

%--------------------------------------------------------------------
%Calulating the thrust (Fx) and levitation (Fy) forces for the HTS

%First conductor (I +ve) Left and Right side of HTS
F1yl = int(int(y/(x^2+y^2),x,x1/1000,x2/1000),y,y1/1000,y2/1000);
F1xl = int(int(x/(x^2+y^2),y,y1/1000,y2/1000),x,x1/1000,x2/1000);
F1yr = -int(int(y/(x^2+y^2),x,x3/1000,x4/1000),y,y1/1000,y2/1000);
F1xr = -int(int(x/(x^2+y^2),y,y1/1000,y2/1000),x,x3/1000,x4/1000);

%Second conductor (I -ve) Left and Right side of HTS
F2yl = -int(int(y/(x^2+y^2),x,(-d1+x1)/1000,(-d1+x2)/1000),y,...
 ...y1/1000,y2/1000);
F2xl = -int(int(x/(x^2+y^2),y,y1/1000,y2/1000),x,...
 ...(-d1+x1)/1000,(-d1+x2)/1000);
F2yr = int(int(y/(x^2+y^2),x,(-d1+x3)/1000,(-d1+x4)/1000),y,...
 ...y1/1000,y2/1000);
F2xr = int(int(x/(x^2+y^2),y,y1/1000,y2/1000),x,...
```

```
 ...(-d1+x3)/1000,(-d1+x4)/1000);

%Sum up the x and y forces
ForceX = (-u*Jc*I/(2*pi))*eval(F1xl+F1xr+F2xl+F2xr);
ForceY = (-u*Jc*I/(2*pi))*eval(F1yl+F1yr+F2yl+F2yr);

%--------------------------------------------------------------------
%                              ##  END  ##
%--------------------------------------------------------------------
%--------------------------------------------------------------------
```

Using this new function it was then possible to produce another function for plotting the change in force with distance. The following script is for a function that plots levitation force versus a change in height (movement along the y-axis) or thrust force versus a change in distance (movement along the x-axis).

```
function pforce = plotforce(a1,b1,a2,b2,w,i,p,f,z)
% PLOTFORCE is a function that plots thrust force against a change in
% x (distance) or levitation force against a change in y (height).
% Thrust versus levitation is also shown.
%
% Forces are calculated (using the CALCFORCE function) moving from a
% given starting point to a specified end point.
% (NOTE: movement is left to right so f > x1)
%
% PLOTFORCE(x1,y1,x2,y2,w,I,p,f,D) where (x1,y1) and (x2,y2) are the
% bottom left and top right co-ordinates of the superconductor area
% carrying current Jc (origin at centre of left conductor), w is the
% width of the superconductor, I is the bulk current in the coil
% (current x turns), p is the coil pitch, f is the final (x or y)
% co-ordinate. D specifies whether distance (1) or height (2) is to
% be varied. [all lengths in mm]
%
%
%                   o(x1,yf) ie D=2
%                              (x2,y2)
%                   .-------o---------.-------.
%                   |  +Jc  |         |  -Jc  |
%                   |       |         |       |
%     y^     (x1,y1)o-------'---------'-------'      o(xf,y1) ie D=1
%      |            |<--------- w ----------->|
%      |
%    __|__                                          ____
%   |  |  |                                       |    |
%   |  *----------->x                              | -I |
%   |  +I |                                       |    |
%    -----                                         ____
%      |<------------------- p ---------------------->|
%
% see also CALCFORCE function
```

```
%-------------------------------------------------------------------------
%                              ##  BEGIN  ##
%-------------------------------------------------------------------------
x=0;
y=0;
px=0;
py=0;

if z==1
   for j=0:1:f-a1
      [fx,fy]=calcforce(a1+j,b1,a2+j,b2,w,i,p);
      x=cat(2,x,a1+j);
      px=cat(2,px,fx);
      py=cat(2,py,fy);
   end
   figure(1);
   plot(x(2:end),px(2:end))
   title('Thrust Force versus Distance');
   xlabel('Distance of SC from coil [mm]');
   ylabel('Thrust Force');
   figure(2);
   plot(x(2:end),py(2:end))
   title('Levitation Force versus Distance');
   xlabel('Distance of SC from coil [mm]');
   ylabel('Levitation Force');

elseif z==2

   for k=0:1:f-b1
      [fx,fy]=calcforce(a1,b1+k,a2,b2+k,w,i,p);
      y=cat(2,y,b1+k);
      px=cat(2,px,fx);
      py=cat(2,py,fy);
   end
   figure(3);
   plot(y(2:end),px(2:end))
   title('Thrust Force versus Height');
   xlabel('Height of SC above coil [mm]');
```

```
   ylabel('Thrust Force [N]');
   figure(4);
   plot(y(2:end),py(2:end))
   title('Levitation Force versus Height');
   xlabel('Height of SC above coil [mm]');
   ylabel('Levitation Force [N]');

else
   error('Incorrect variable assignment. D = 1 for movement along
   x-axis or D = 2 for movement along y-axis.')
end

%-------------------------------------------------------------------
%                            ##  END  ##
%-------------------------------------------------------------------
%-------------------------------------------------------------------
```

B.2 3-Phases and Two Rows of HTSs

The final MATLAB™ script produced is for a function which calculates the thrust forces between a MagLev vehicle containing two rows of bulk HTSs and a 3-phase sinusoidal supply. This script takes the resulting MMF wave of the 3-phase supply into account when working out the force integrals. Furthermore it provides results for two vehicle topologies namely one pole-pitch and half a pole-pitch spacing between HTS rows.

```
function [tot1,tot2] = HTSforce(a1,b1,a2,w,p,i,f,n)
% [F1,F2] = HTSFORCE is a function that calculates the thrust forces
% developed between a Linear Motor 3-phase winding and a MagLev
% vehicle containing two rows of bulk superconducting pellets separa-
% ted by either one pole-pitch or half a pole-pitch. (Movement along
% x-axis)
%
% [A,B] = HTSFORCE(x1,y1,x2,w,p,I,f,n) where (x1,y1) and (x2,y2)
% are the bottom left and top right co-ordinates of superconductor
% area carrying current Jc (origin at centre of left conductor), w is
% the superconductor width, I is the bulk coil current [A](current
% x turns), f is the frequency of the supply in [Hz], n is the number
% of time intervals to use and p is the distance between coil sides
% (coil pitch).
% [all length units in mm]
%
% This Program Returns:
% A = thrust force for vehicle with one pole-pitch spacing
% B = thrust force for vehicle with half a pole-pitch spacing
%
% Also produces plots of calculated forces for one cycle of the
% specified frequency.
% Plots:
%       I) Thrust Force versus Time (HTSs 1 pole-pitch apart)
%       II) Thrust Force versus Time (HTSs 1/2 pole-pitch apart)
%       III) I and II as subplots on same figure
%       IV) I and II on same axes
%
%
%
```

```
%                                    (x2,y2)
%                            .-------o---------.-------.
%                            |  +Jc  |         |  -Jc  |
%                            |       |         |       |
%               y^     (x1,y1)o-------'---------'-------'
%                |            |<--------- w ----------->|
%                |
%              __|__                                        ____
%             |  |  |                                      |    |
%             |  *----------->x                             | -I |
%             |  +I |                                       |    |
%              -----                                        ____
%                |<------------------- p --------------------->|
%                -   -   -   -   -   -   -   -   -   -
% Phase layout:| |A| |b| |C| |a| |B| |c| |A| |b| |C| |
%               | |_| |_| |_| |_| |_| |_| |_| |_| |_| |
%               |_____________________________________|
%
% e.g. [OnePole,HalfPole] = htsforce(5,1,9,20,57,450,10,300);;
%                                                    ^
%                                                    5A * 90turns
%
```

```
%--------------------------------------------------------------------
%                            #  BEGIN  #
%--------------------------------------------------------------------
%
%####################################################################
%                     CONSTANTS AND VARIABLES
%####################################################################
syms x y;
s=@sum;
u=pi*4*1e-7; %permeability of air
Jc=1e7;     % HTS critical current density
%---------------------------------------
%       3-Phase Supply Variables
%---------------------------------------
%frequency
T=1/f;
```

```
t=transpose([0:(3*T/2)/(n-1):3*T/2]);
time=t(1:2*n/3);
%3 phases
A = (sin((2*pi*f*t)-5*pi/3));
b = (sin(2*pi*f*t));
C = (sin((2*pi*f*t)-pi/3));
Ip = i*sqrt(2); % peak = RMS x sqrt(2)
IA = (Ip)*(A);
Ib = (Ip)*(b);
IC = (Ip)*(C);
mmf = (IA+Ib+IC);
norm_mmf = mmf(1:2*n/3);
%---------------------------------------
%       Dimension Variables
%---------------------------------------
% percentage of HTS used for Jc (100% = quenched HTS)
per=(2*(a2-a1)/w)*100;
sl = 19; % distance between centre of 2 adjacent coils
d1 = p;   % LM pole-pitch
lz = 0.1; % length of the HTSs into the plane (width of LM)
%y co-ords for all HTSs
y1 = b1;
y2 = y1+12;
%x co-ords for first HTS
x1 = a1;
x2 = a2;
x4 = x1+w;
x3 = x4-(x2-x1);
%x co-ords for 2nd HTS one pp away
x5=x1+d1;
x6=x2+d1;
x7=x3+d1;
x8=x4+d1;
%x co-ords for 2nd HTS half a pp away
x9=x1+(d1/2);
x10=x2+(d1/2);
x11=x3+(d1/2);
x12=x4+(d1/2);
```

```
%#####################################################################
%                   CALCULATE INTEGRATION CONSTANTS
%#####################################################################
%constants for first HTS and second HTS (one pp away)
kA=[];
kb=[];
kC=[];
for j=1:(2*n/3)
    if mmf(j) >= 0
        kA(end+1) = -(u*Jc*IA(j)*lz/(2*pi));
        kb(end+1) = -(u*Jc*Ib(j)*lz/(2*pi));
        kC(end+1) = -(u*Jc*IC(j)*lz/(2*pi));
    else
        kA(end+1) = (u*Jc*IA(j)*lz/(2*pi));
        kb(end+1) = (u*Jc*Ib(j)*lz/(2*pi));
        kC(end+1) = (u*Jc*IC(j)*lz/(2*pi));
    end
end

%constants for second HTS half a pp away
kAh=[];
kbh=[];
kCh=[];
for j=1:(2*n/3)
    if j <= n/6
        kAh(end+1) = -(u*Jc*IA(j+n/6)*lz/(2*pi));
        kbh(end+1) = -(u*Jc*Ib(j+n/6)*lz/(2*pi));
        kCh(end+1) = -(u*Jc*IC(j+n/6)*lz/(2*pi));
    elseif ((j > n/6) & (j <= n/2))
        kAh(end+1) = (u*Jc*IA(j+n/6)*lz/(2*pi));
        kbh(end+1) = (u*Jc*Ib(j+n/6)*lz/(2*pi));
        kCh(end+1) = (u*Jc*IC(j+n/6)*lz/(2*pi));
    else
        kAh(end+1) = -(u*Jc*IA(j+n/6)*lz/(2*pi));
        kbh(end+1) = -(u*Jc*Ib(j+n/6)*lz/(2*pi));
        kCh(end+1) = -(u*Jc*IC(j+n/6)*lz/(2*pi));
    end
end
```

```
%#####################################################################
%          CALCULATING FORCE INTEGRALS FOR EACH PHASE CURRENT
%#####################################################################
%---------------------------------------------------------------------
% first HTS
%---------------------------------------------------------------------

%in coil
    %left side of HTS
    FA_in_left = int(int(x/(x^2+y^2),y,y1/1000,y2/1000),x,...
...(x1)/1000,(x2)/1000);
    Fb_in_left = int(int(x/(x^2+y^2),y,y1/1000,y2/1000),x,...
...(x1-sl)/1000,(x2-sl)/1000);
    FC_in_left = int(int(x/(x^2+y^2),y,y1/1000,y2/1000),x,...
...(x1-2*sl)/1000,(x2-2*sl)/1000);

    %right side of HTS (-ve sign because Jz is negative)
    FA_in_right = -int(int(x/(x^2+y^2),y,y1/1000,y2/1000),x,...
...(x3)/1000,(x4)/1000);
    Fb_in_right = -int(int(x/(x^2+y^2),y,y1/1000,y2/1000),x,...
...(x3-sl)/1000,(x4-sl)/1000);
    FC_in_right = -int(int(x/(x^2+y^2),y,y1/1000,y2/1000),x,...
...(x3-2*sl)/1000,(x4-2*sl)/1000);

%out (return) coil

%Added -ve sign because curretn I(t) is in opposite direction, this
%way don't need to change k (can use those calculated for 'in coil')
    %left side of HTS
    FA_out_left = -(int(int(x/(x^2+y^2),y,y1/1000,y2/1000),x,...
...(x1-d1)/1000,(x2-d1)/1000));
    Fb_out_left = -(int(int(x/(x^2+y^2),y,y1/1000,y2/1000),x,...
...(x1-sl-d1)/1000,(x2-sl-d1)/1000));
    FC_out_left = -(int(int(x/(x^2+y^2),y,y1/1000,y2/1000),x,...
...(x1-2*sl-d1)/1000,(x2-2*sl-d1)/1000));

    %right side of HTS (-ve sign because Jz is negative)
    FA_out_right = -(-int(int(x/(x^2+y^2),y,y1/1000,y2/1000),x,...
```

```
...(x3-d1)/1000,(x4-d1)/1000));
    Fb_out_right = -(-int(int(x/(x^2+y^2),y,y1/1000,y2/1000),x,...
...(x3-sl-d1)/1000,(x4-sl-d1)/1000));
    FC_out_right = -(-int(int(x/(x^2+y^2),y,y1/1000,y2/1000),x,...
...(x3-2*sl-d1)/1000,(x4-2*sl-d1)/1000));

%-----------------------------------------------------------------------
% second HTS (one pp away from 1st HTS)
%-----------------------------------------------------------------------

%in coil
    %left side of HTS (for opp away, HTS is in the -ve B field so Jz
    %flows in opposite direction i.e. Jz is -ve on left side)
    %-ve sign here allows use of same k as for first HTS
    FA_in_left_op = -int(int(x/(x^2+y^2),y,y1/1000,y2/1000),x,...
...(x5)/1000,(x6)/1000);
    Fb_in_left_op = -int(int(x/(x^2+y^2),y,y1/1000,y2/1000),x,...
...(x5-sl)/1000,(x6-sl)/1000);
    FC_in_left_op = -int(int(x/(x^2+y^2),y,y1/1000,y2/1000),x,...
...(x5-2*sl)/1000,(x6-2*sl)/1000);

    %right side of HTS (removed -ve because Jz is +ve on right side)
    FA_in_right_op = int(int(x/(x^2+y^2),y,y1/1000,y2/1000),x,...
...(x7)/1000,(x8)/1000);
    Fb_in_right_op = int(int(x/(x^2+y^2),y,y1/1000,y2/1000),x,...
...(x7-sl)/1000,(x8-sl)/1000);
    FC_in_right_op = int(int(x/(x^2+y^2),y,y1/1000,y2/1000),x,...
...(x7-2*sl)/1000,(x8-2*sl)/1000);

% out (return) coil
    %Added -ve sign because curretn I(t) is in opposite direction
    %left side of HTS
    FA_out_left_op = -(-int(int(x/(x^2+y^2),y,y1/1000,y2/1000),x,...
...(x5-d1)/1000,(x6-d1)/1000));
    Fb_out_left_op = -(-int(int(x/(x^2+y^2),y,y1/1000,y2/1000),x,...
...(x5-sl-d1)/1000,(x6-sl-d1)/1000));
    FC_out_left_op = -(-int(int(x/(x^2+y^2),y,y1/1000,y2/1000),x,...
...(x5-2*sl-d1)/1000,(x6-2*sl-d1)/1000));
```

```
    %right side of HTS
    FA_out_right_op = -(int(int(x/(x^2+y^2),y,y1/1000,y2/1000),x,...
...(x7-d1)/1000,(x8-d1)/1000));
    Fb_out_right_op = -(int(int(x/(x^2+y^2),y,y1/1000,y2/1000),x,...
...(x7-sl-d1)/1000,(x8-sl-d1)/1000));
    FC_out_right_op = -(int(int(x/(x^2+y^2),y,y1/1000,y2/1000),x,...
...(x7-2*sl-d1)/1000,(x8-2*sl-d1)/1000));

%-----------------------------------------------------------------------
% second HTS (half a pp away from 1st HTS)
%-----------------------------------------------------------------------

%in coil
    %left side of HTS
    FA_in_left_ohp = int(int(x/(x^2+y^2),y,y1/1000,y2/1000),x,...
...(x9)/1000,(x10)/1000);
    Fb_in_left_ohp = int(int(x/(x^2+y^2),y,y1/1000,y2/1000),x,...
...(x9-sl)/1000,(x10-sl)/1000);
    FC_in_left_ohp = int(int(x/(x^2+y^2),y,y1/1000,y2/1000),x,...
...(x9-2*sl)/1000,(x10-2*sl)/1000);

    %right side of HTS (-ve sign because Jz is in opposite direction)
    FA_in_right_ohp = -int(int(x/(x^2+y^2),y,y1/1000,y2/1000),x,...
...(x11)/1000,(x12)/1000);
    Fb_in_right_ohp = -int(int(x/(x^2+y^2),y,y1/1000,y2/1000),x,...
...(x11-sl)/1000,(x12-sl)/1000);
    FC_in_right_ohp = -int(int(x/(x^2+y^2),y,y1/1000,y2/1000),x,...
...(x11-2*sl)/1000,(x12-2*sl)/1000);

%out (return) coil

%Added -ve sign because curretn I(t) is in opposite direction, this
%way don't need to change kh (can use those calculated for in coil)

    %left side of HTS
    FA_out_left_ohp = -(int(int(x/(x^2+y^2),y,y1/1000,y2/1000),x,...
...(x9-d1)/1000,(x10-d1)/1000));
    Fb_out_left_ohp = -(int(int(x/(x^2+y^2),y,y1/1000,y2/1000),x,...
...(x9-sl-d1)/1000,(x10-sl-d1)/1000));
```

```
    FC_out_left_ohp = -(int(int(x/(x^2+y^2),y,y1/1000,y2/1000),x,...
...(x9-2*sl-d1)/1000,(x10-2*sl-d1)/1000));

    %right side of HTS (-ve sign because Jz is in opposite direction)
   FA_out_right_ohp = -(-int(int(x/(x^2+y^2),y,y1/1000,y2/1000),x,...
...(x11-d1)/1000,(x12-d1)/1000));
   Fb_out_right_ohp = -(-int(int(x/(x^2+y^2),y,y1/1000,y2/1000),x,...
...(x11-sl-d1)/1000,(x12-sl-d1)/1000));
   FC_out_right_ohp = -(-int(int(x/(x^2+y^2),y,y1/1000,y2/1000),x,...
...(x11-2*sl-d1)/1000,(x12-2*sl-d1)/1000));


%#########################################################################
%                   ADD RESULTS OF EACH INTEGRATION
%#########################################################################

%Sum up the forces for first HTS
Force_A = feval(s,[FA_in_left FA_in_right FA_out_left FA_out_right]);
Force_b = feval(s,[Fb_in_left Fb_in_right Fb_out_left Fb_out_right]);
Force_C = feval(s,[FC_in_left FC_in_right FC_out_left FC_out_right]);

%Sum up the forces for second HTS (opp away from 1st HTS)
Force_A_op = feval(s,[FA_in_left_op FA_in_right_op FA_out_left_op...
...FA_out_right_op]);
Force_b_op = feval(s,[Fb_in_left_op Fb_in_right_op Fb_out_left_op...
...Fb_out_right_op]);
Force_C_op = feval(s,[FC_in_left_op FC_in_right_op FC_out_left_op...
...FC_out_right_op]);

%Sum up the forces for second HTS (half a pp away from 1st HTS)
Force_A_ohp = feval(s,[FA_in_left_ohp FA_in_right_ohp...
...FA_out_left_ohp FA_out_right_ohp]);
Force_b_ohp = feval(s,[Fb_in_left_ohp Fb_in_right_ohp...
...Fb_out_left_ohp Fb_out_right_ohp]);
Force_C_ohp = feval(s,[FC_in_left_ohp FC_in_right_ohp...
...FC_out_left_ohp FC_out_right_ohp]);

%-------------------------------------------------------------------------
% evaluate totals for each phase and each HTS row
```

```
% (multiply integral solutions by appropriate integration constant)
%-----------------------------------------------------------------------
%1st HTS
Total_A_1st = kA*eval(Force_A);
Total_b_1st = kb*eval(Force_b);
Total_C_1st = kC*eval(Force_C);
Total_1st = Total_A_1st + Total_b_1st + Total_C_1st;

%2nd HTS one pp away
Total_A_2nd_op = kA*eval(Force_A_op);
Total_b_2nd_op = kb*eval(Force_b_op);
Total_C_2nd_op = kC*eval(Force_C_op);
Total_2nd_op = Total_A_2nd_op + Total_b_2nd_op + Total_C_2nd_op;

%2nd HTS half a pp away
Total_A_2nd_ohp = kAh*eval(Force_A_ohp);
Total_b_2nd_ohp = kbh*eval(Force_b_ohp);
Total_C_2nd_ohp = kCh*eval(Force_C_ohp);
Total_2nd_ohp = Total_A_2nd_ohp + Total_b_2nd_ohp + Total_C_2nd_ohp;

%-----------------------------------------------------------------------
% Total thrust forcese for for each vehicle
%-----------------------------------------------------------------------
%HTSs one pole-pitch apart
    tot1 = Total_1st + Total_2nd_op;

%HTSs half a pole-pitch apart
    tot2 = Total_1st + Total_2nd_ohp;


%#######################################################################
%                            PLOT RESULTS
%#######################################################################

%first set up some handy variables
mid=mean(t);
z=zeros(2*n/3,1);
percent=[num2str(per),'% of HTS carrying current'];
%work out the RMS values
```

```
rms_op = norm(tot1)/sqrt(200);
rms1=ones(2*n/3,1)*rms_op;
rms_ohp = norm(tot2)/sqrt(200);
rms2=ones(2*n/3,1)*rms_ohp;
rms_labe1_op=['RMS_{1pp} = ',num2str(rms_op)];
rms_labe1_ohp=['RMS_{1/2pp} = ',num2str(rms_ohp)];

% plot force for HTSs 1pp apart
figure;
plot(time,tot1,time,rms1)
grid;
Xlim ([0 T]);
title(['Thrust Force versus Time (1 pp) with ',percent,' at ',...
...num2str(f),'Hz']);
ylabel('Thrust Force [N]');
xlabel('Time [s]');
text(mid,rms_op,rms_labe1_op,...
    'HorizontalAlignment','center','FontSize',13)
axis tight;
% plot force for HTSs 1/2pp apart
figure;
plot(time,tot2,time,rms2)
Xlim ([0 T]);
title(['Thrust Force versus Time (^1/_2 pp) with ',percent,' at ',...
...num2str(f),'Hz']);
ylabel('Thrust Force [N]');
xlabel('Time [s]');
%write RMS value on graph
text(mid,rms_ohp,rms_labe1_ohp,...
    'HorizontalAlignment','center','FontSize',13)
grid;
axis tight;

% plot forces for 1pp and 1/2pp HTSs on same figure as subplots
figure;
subplot(2,1,1),plot(time,tot1,time,rms1,time,z,'k')
text(mid,rms_op,rms_labe1_op,...
    'HorizontalAlignment','center','FontSize',13)
grid;
```

```
Xlim ([0 T]);
title(['Thrust Forces versus Time with ',percent,' at ',...
...num2str(f),'Hz']);
ylabel('1 pp Thrust Force [N]');
subplot(2,1,2),plot(time,tot2,time,rms2,time,z,'k')
ylabel('^1/_2 pp Thrust Force [N]');
xlabel('Time [s]');
text(mid,rms_ohp,rms_labe1_ohp,...
    'HorizontalAlignment','center','FontSize',13)
grid;
axis tight;

% plot forces for 1pp and 1/2pp HTSs on same axes
figure;
plot(time,tot1,time,rms1,time,tot2,time,rms2)
Xlim ([0 T]);
title(['1 pp and ^1/_2 pp Thrust Forces versus Time with',percent,...
...' at ',num2str(f),'Hz']);
ylabel('Thrust Force [N]');
xlabel('Time [s]');
legend('1 pp',rms_labe1_op,'1/2 pp',rms_labe1_ohp,-1);
grid;

%------------------------------------------------------------------------
%                            ##  END  ##
%------------------------------------------------------------------------
%------------------------------------------------------------------------
```

Appendix C

Plots of Analytical Results

C.1 Frequency Simulations

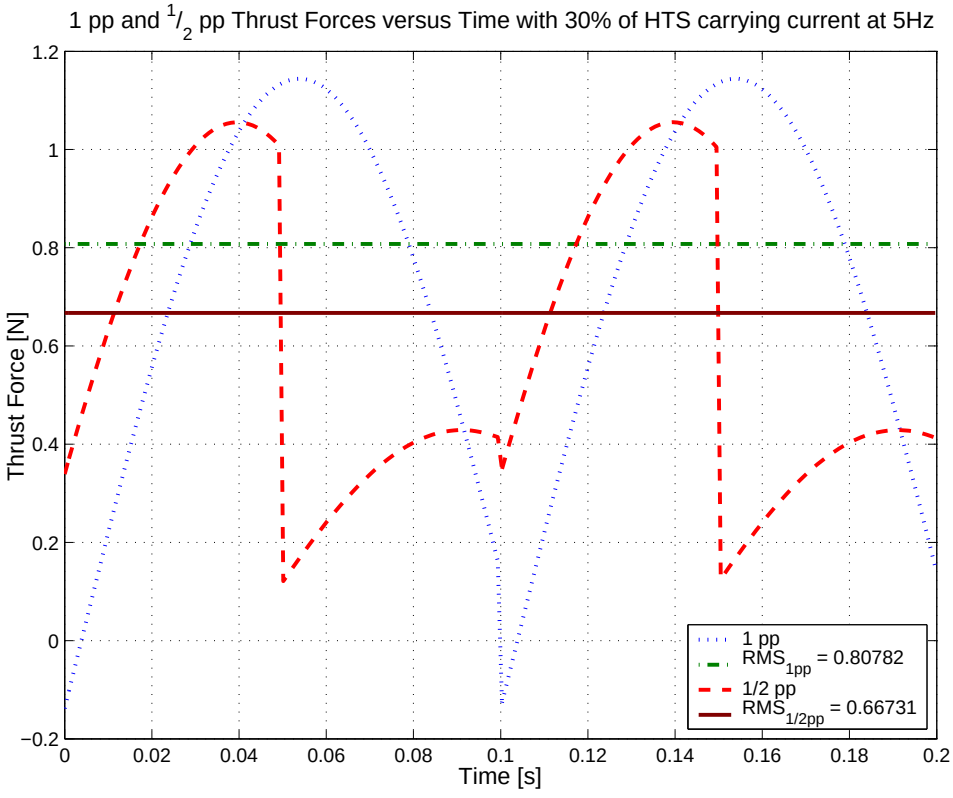

(a)

Figure C.1 Thrust Forces (with 30% of HTS Used) at: (a) 5 Hz

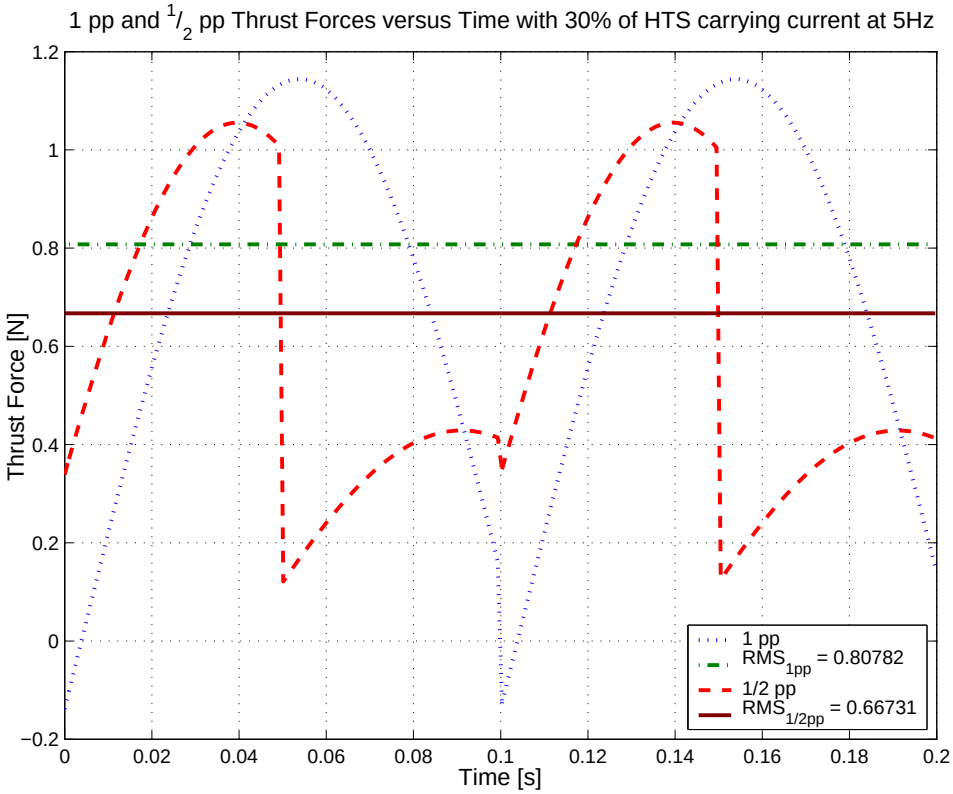

(b)

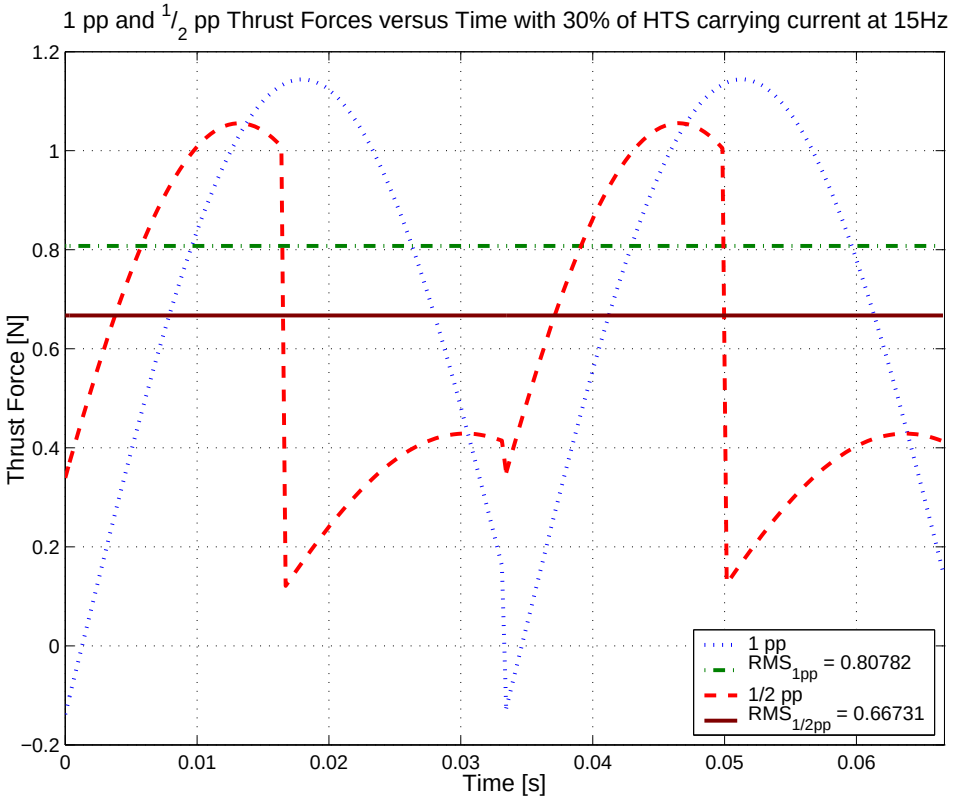

(c)

Figure C.1 (Continued)

(b) 10 Hz and (c) 15 Hz

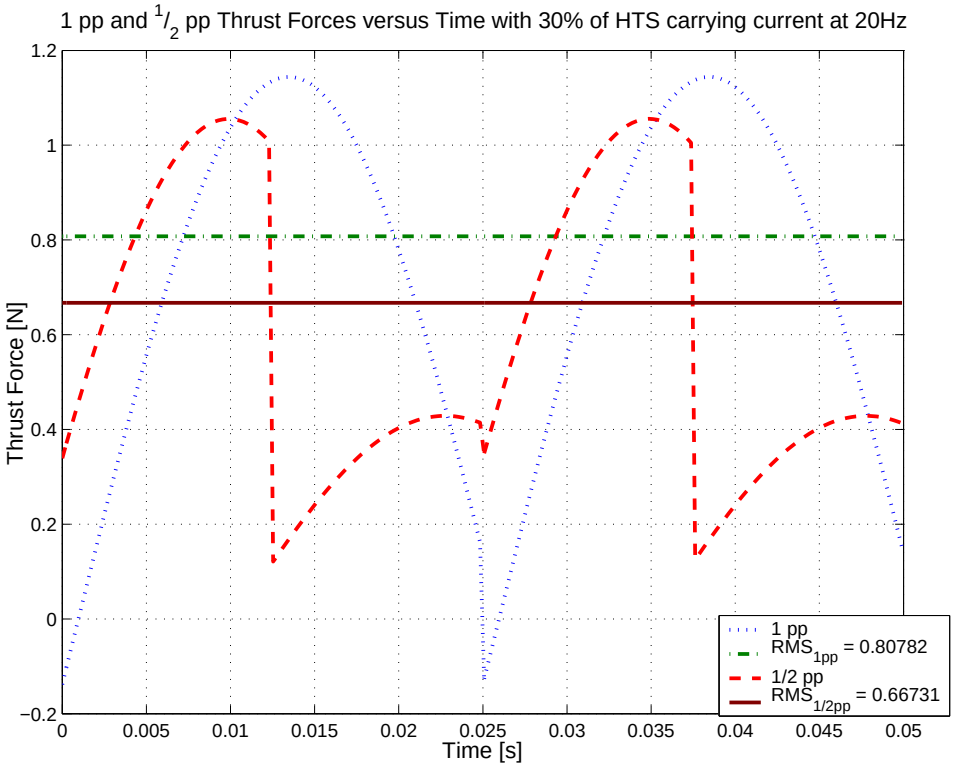

(d)

Figure C.1 (Continued)

(d) 20 Hz.

Analytical calculations showed that changing only the frequency variable had no effect on the resultant thrust forces produced except for changing the period of the waveform i.e. increasing the speed of the MagLev vehicle. Figures C.1 (a) to C.1 (d) show the calculated thrust forces for both vehicle topologies (1 and $\frac{1}{2}$ pole-pitch) for various frequencies but with the same percentage of flux penetration.

Although the period of the waves differs, the magnitude of the forces for both the 1 pole-pitch and $\frac{1}{2}$ pole-pitch layouts remains the same at each frequency with 30% penetration.

C.2 Varying Percentage Penetration

The MATLAB™ script written to perform the analytical calculations, allows the user to vary the amount of HTS area to be used for carrying the "supper-current" of density J_c. Unfortunately due to the error introduced by the arctangent as the integration limits approach the origin of the conductors, it was not possible to calculated the full range of penetration percentages (0% to 100%). This problem was more evident in the $\frac{1}{2}$ pole-pitch layout since the smaller space between the HTSs allowed for less increase in integration area before reaching the error region.

Figures C.2 (a) to C.2 (e) show the effect of increasing the percentage penetration from 10% to 44.9%. These results are for both the 1 pole-pitch and $\frac{1}{2}$ pole-pitch topologies and are all run at 10 Hz.

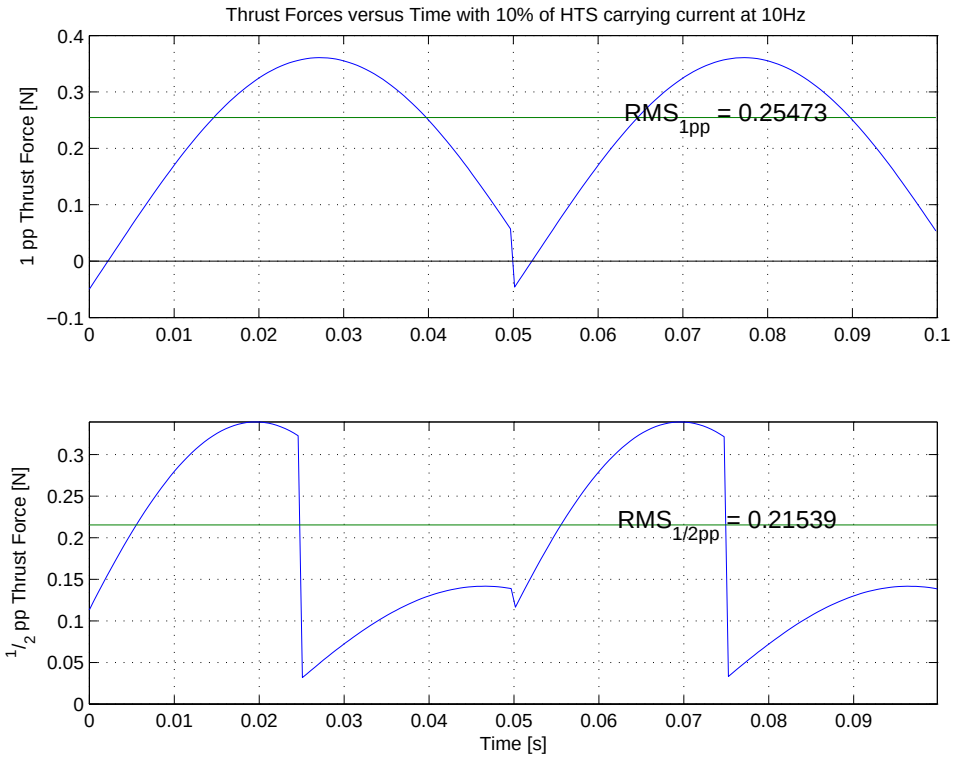

(a)

Figure C.2 Thrust Forces (at 10 Hz) with: (a) 10%, of HTS Used.

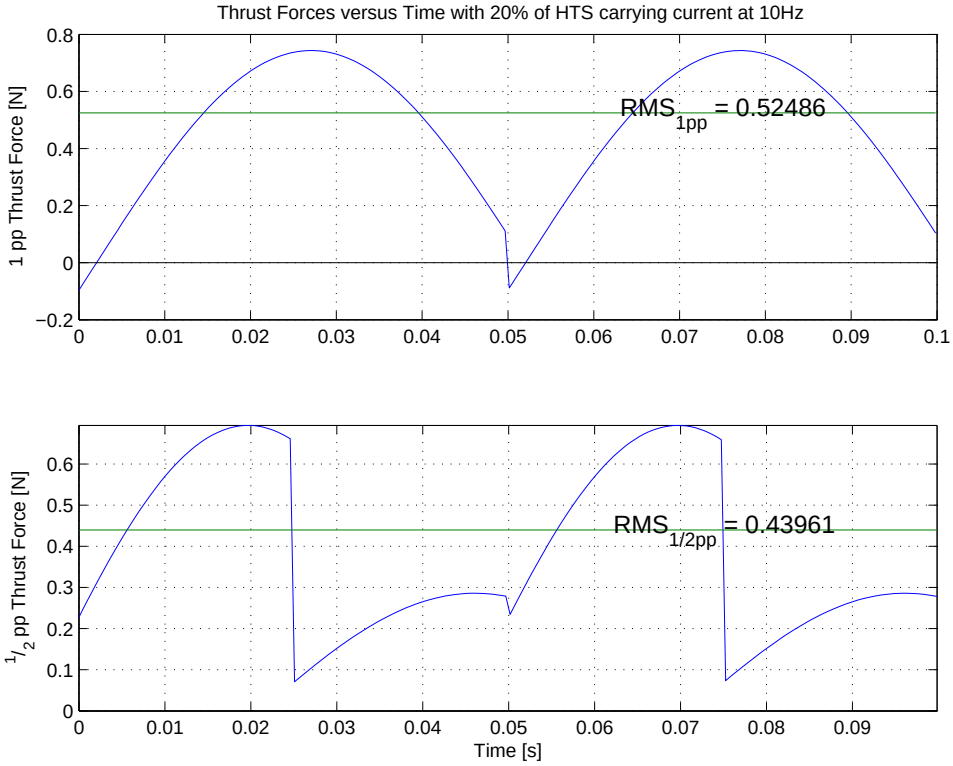

(b)

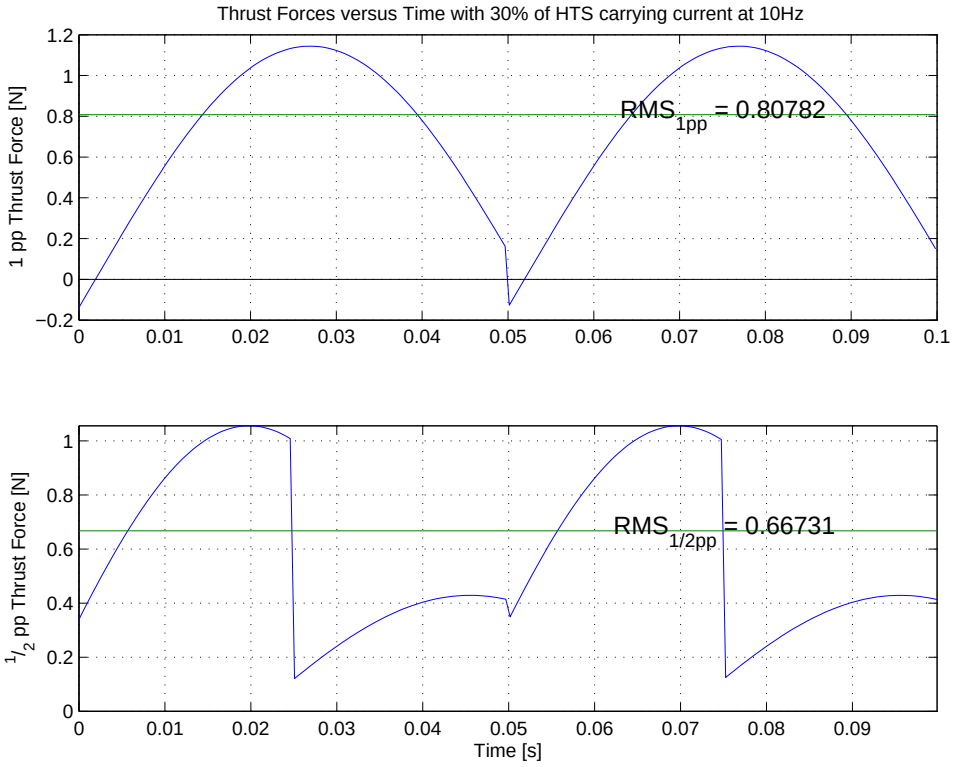

(c)

Figure C.2 (Continued)

(b) 20%, and (c) 30%, of HTS Used.

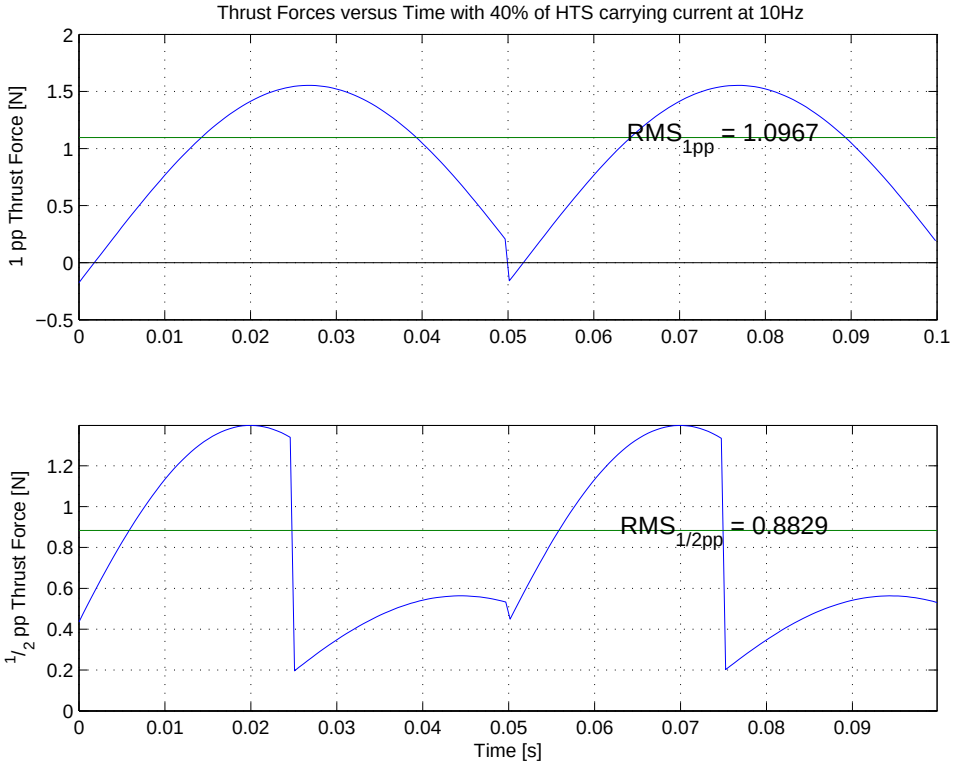

(d)

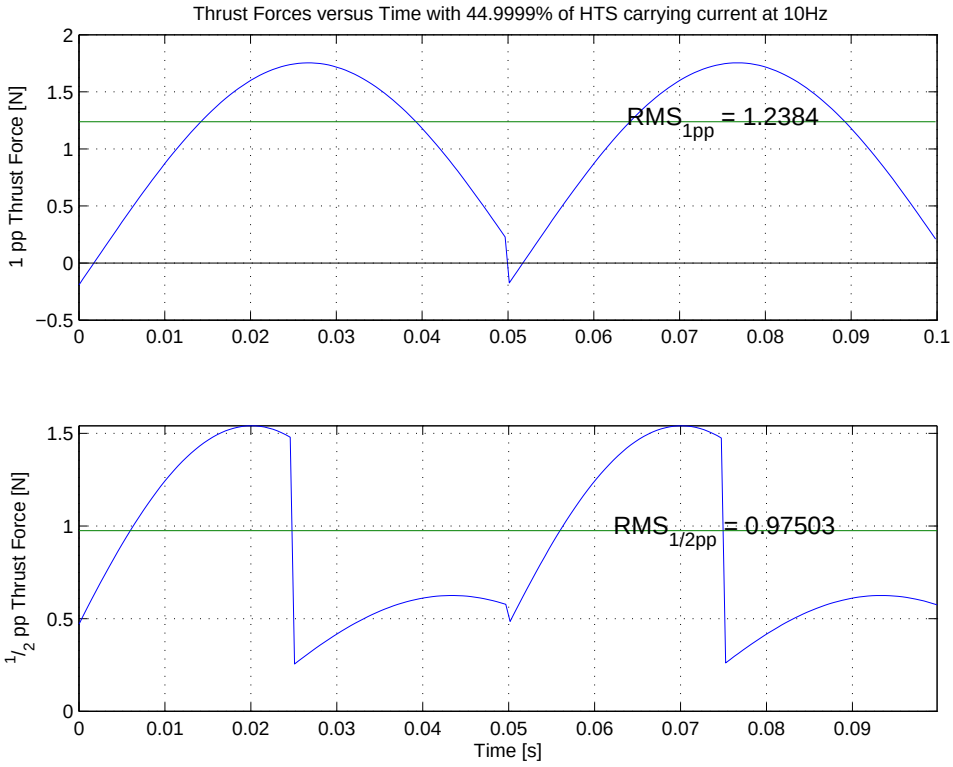

(e)

Figure C.2 (Continued)

(d) 40%, and (e) 44.9%, of HTS Used.

From these figures it is clear that the thrust forces for both layouts increase as the percentage of HTS area used to transport current increases. Furthermore the difference between the 1 pole-pitch and $\frac{1}{2}$ pole-pitch forces increases with increasing flux penetration. If the forces are plotted against the amount of penetration, the 1 pole-pitch forces are seen to have a steeper gradient than the $\frac{1}{2}$ pole-pitch results (see Figure 5.1).

The reason for using 44.99% penetration in figure C.2 (e) is that the arctangent error starts at 45% for the $\frac{1}{2}$ pole-pitch layout. However, it is possible to calculate further penetration for the 1 pole-pitch layout. Figures C.3 (a) to C.3 (f) show the calculated thrust forces for the 1 pole-pitch HTS separation from 50% to 99.9%.

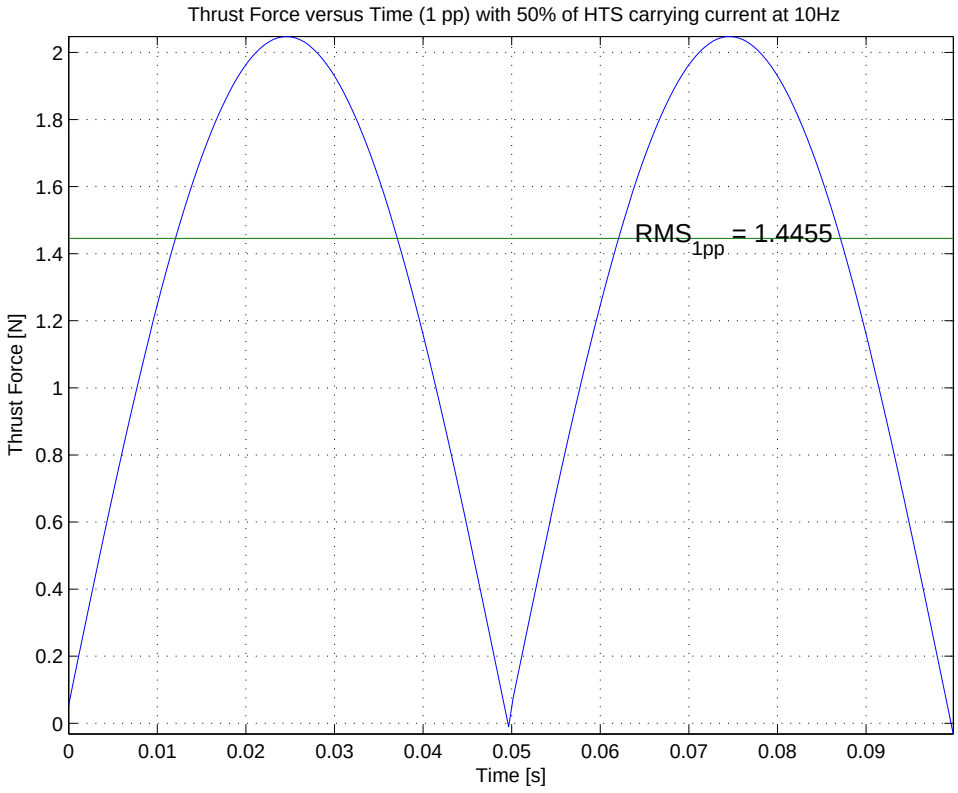

(a)

Figure C.3 Thrust Forces (1 pole-pitch layout at 10 Hz) with: (a) 50%, of HTS Used.

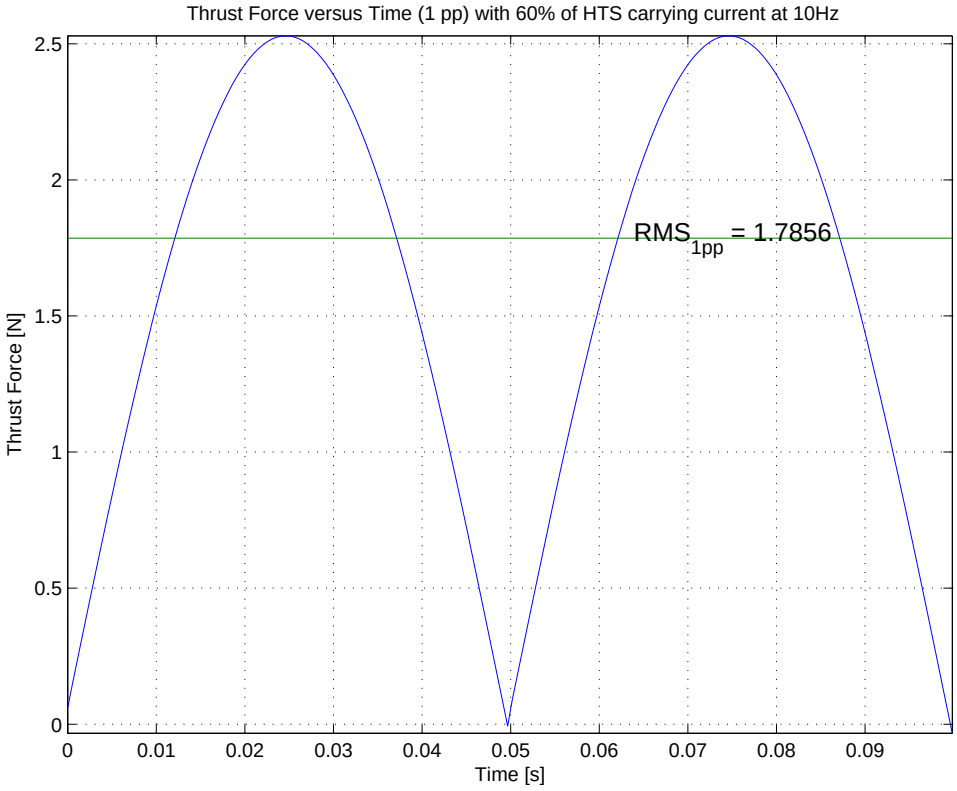

(b)

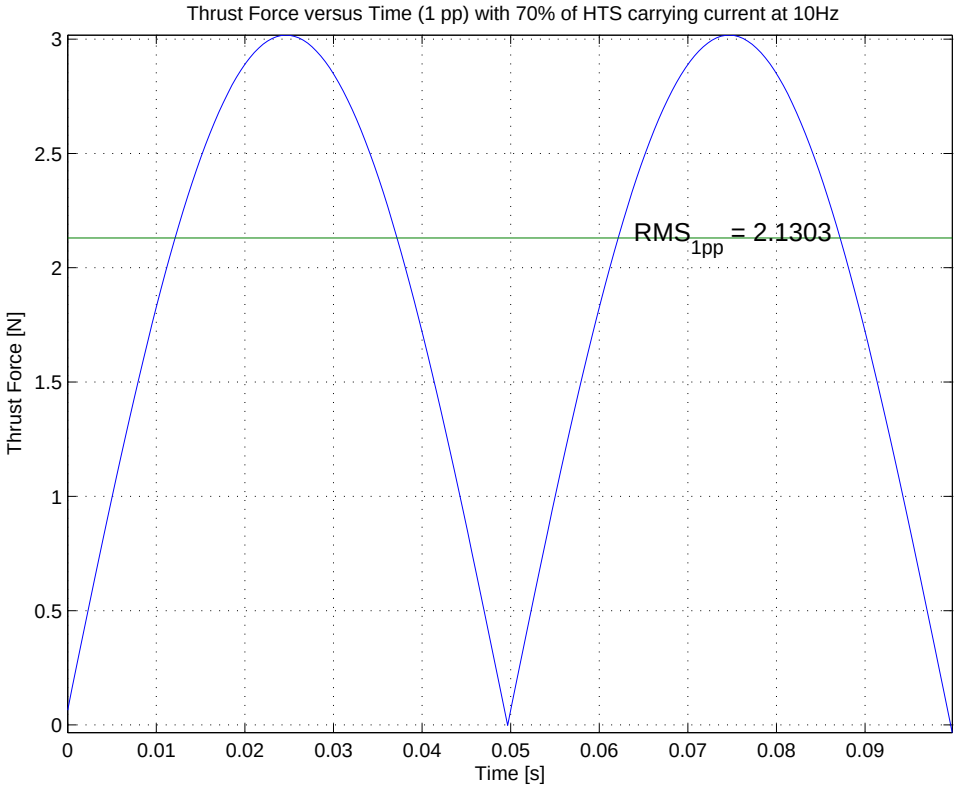

(c)

Figure C.3 (Continued)

(b) 60%, (c) 70%, of HTS Used.

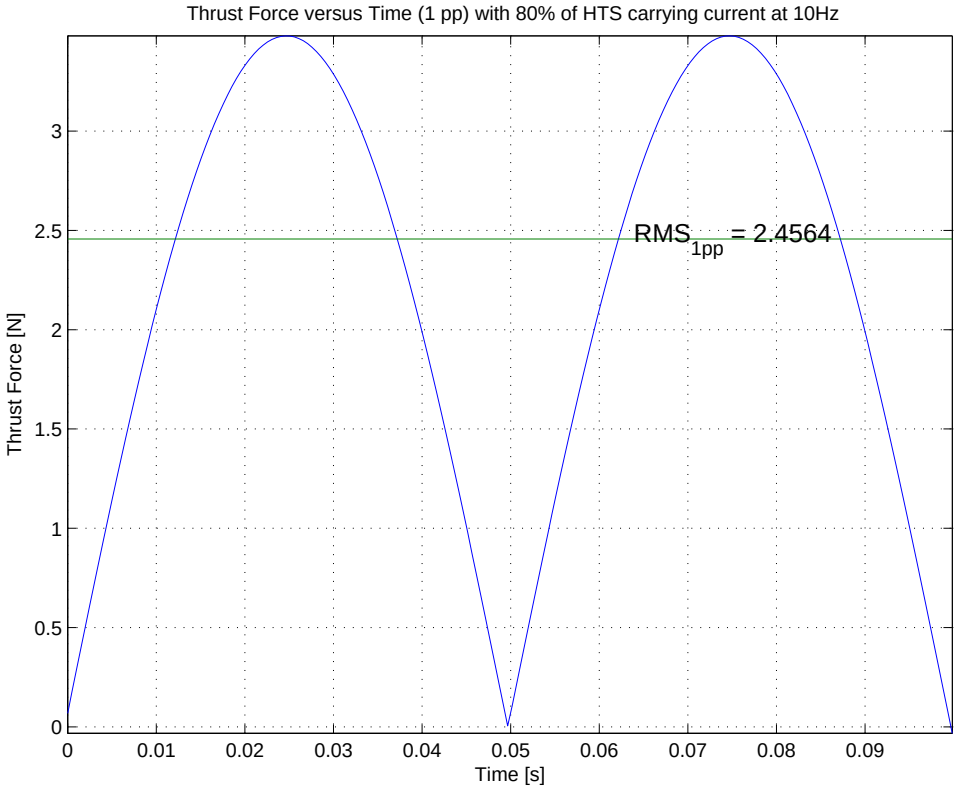

(d)

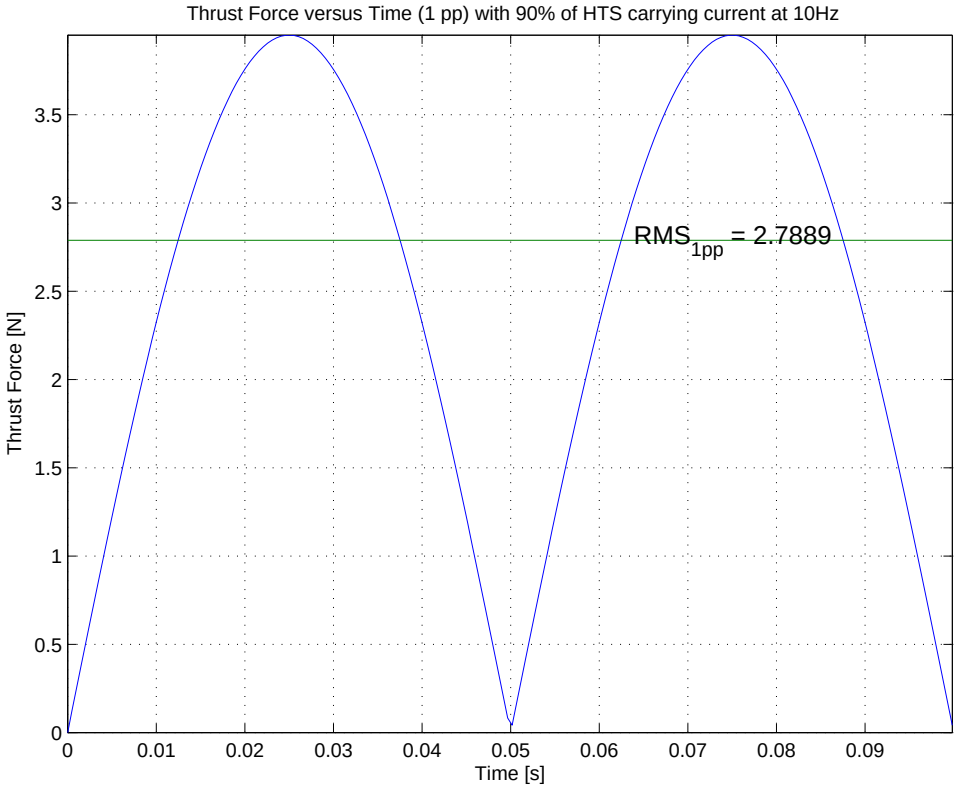

(e)

Figure C.3 (Continued)

(d) 80%, (e) 90%, of HTS Used.

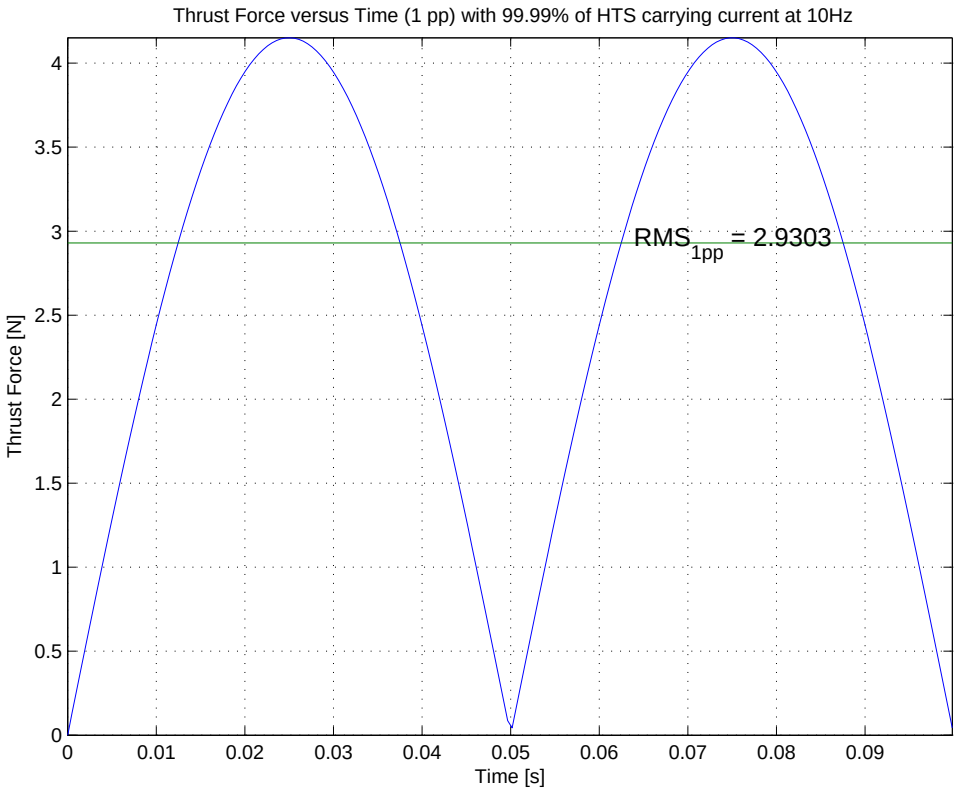

(f)

Figure C.3 (Continued)

and (f) 99%, of HTS Used.

For the layout with 1 pole-pitch spacing between HTS rows it was possible to increase the size of the integration area until 99.9% before any errors occured. It should be noted that the error is dependent on the starting co-ordinate of the HTS relative to the coil. Also at 100% penetration the HTS saturates and instantly returns to a normal non-superconducting state.

Appendix D

Liquid Nitrogen Safety Procedures

WARNING !! Liquid Nitrogen must be handled with care. If mishandled it can cause **Frostbite**, **Eye Damage**, **Torn Flesh**, or **Asphyxiation**.

D.1 General Precautions

1. Wear Protective Clothing
    - Hand protection such as thick loose gloves.
    - Goggles or face shield to protect eyes.
    - Long pants, apron or overall.
    - Closed shoes.
2. Use in Well Ventilated Area
    - Although Nitrogen is not poisonous, if sufficient liquid nitrogen is vaporised it can displace enough Oxygen to cause dangerous levels of below 20% Oxygen to 100% Nitrogen.
    - This can cause **Asphyxiation**.
3. Storing Liquid Nitrogen
    - Use Dewars designed for extreme cold: well insulated and can handle thermal stress.
    - Never seal the container as this will lead to pressure buildup and could cause the container to burst violently.
    - Cover with ventilated lid

4. Handling

    - Many materials become brittle when exposed to Liquid Nitrogen and may break into sharp pieces.
    - Avoid using glass or plastic containers unless designed for extreme cold.
    - Some commonly used materials are: styrofoam, stainless steel, aluminum, brass, copper, pyrex, wood, paper, cardboard, masking tape, cotton thread, and teflon.

D.2 Treatment of Frostbite

1. **Immediately** flood or submerge affected area in clean, unheated water.
2. Remove any clothing that may restrict flow of blood to the affected area.
3. If eyes are affected, skin is blistered, or frostbite is extensive or severe, **Seek Medical Attention Immediately**.

Appendix E

Vehicle Design Details

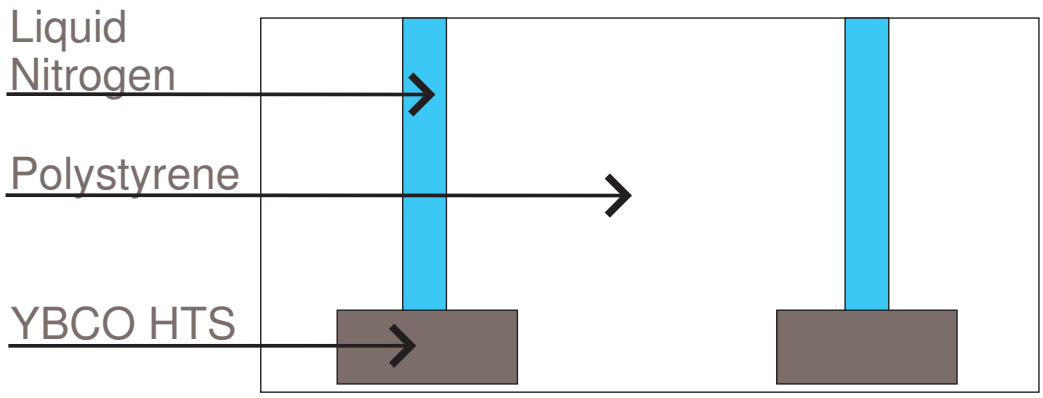

Figure E.1 Materials Used for Vehicle Design

Figure E.1 shows the different materials used in the design of the MagLev vehicle. The following sections contain drawings, with dimensions, of both the 1 pole-pitch and $1^1/_2$ pole-pitch MagLev vehicles used for testing. The $1^1/_2$ pole-pitch spacing was used instead of the $^1/_2$ pole-pitch spacing for practical design reasons. Drawings and dimensions of the bulk YBCO Levitators^{TM} used are also provided. Note that all dimensions are in millimetres (mm) and that drawings are not drawn to scale.

E.1 YBCO Pellets

Figure E.2 shows the shape and size of the bulk HTSs used for experimentation. Each vehicle contained ten of these pellets (two rows of five).

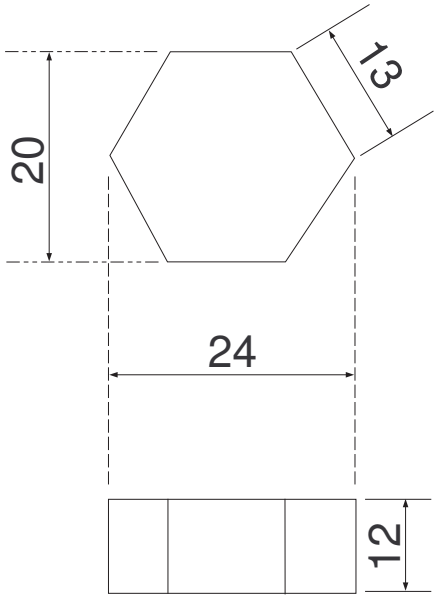

Figure E.2 Dimensions of Bulk YBCO Pellets

E.2 One Pole Pitch Vehicle

Figures E.3 and E.4 show the top view and side view of the 1 pole-pitch vehicle with dimensions.

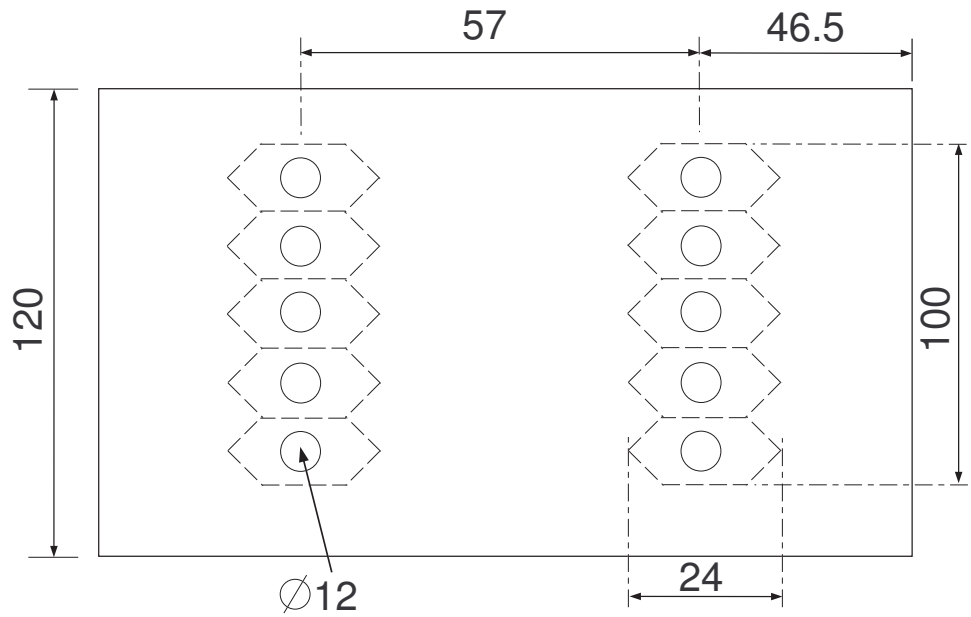

Figure E.3 Top View of 1 pole-pitch Vehicle

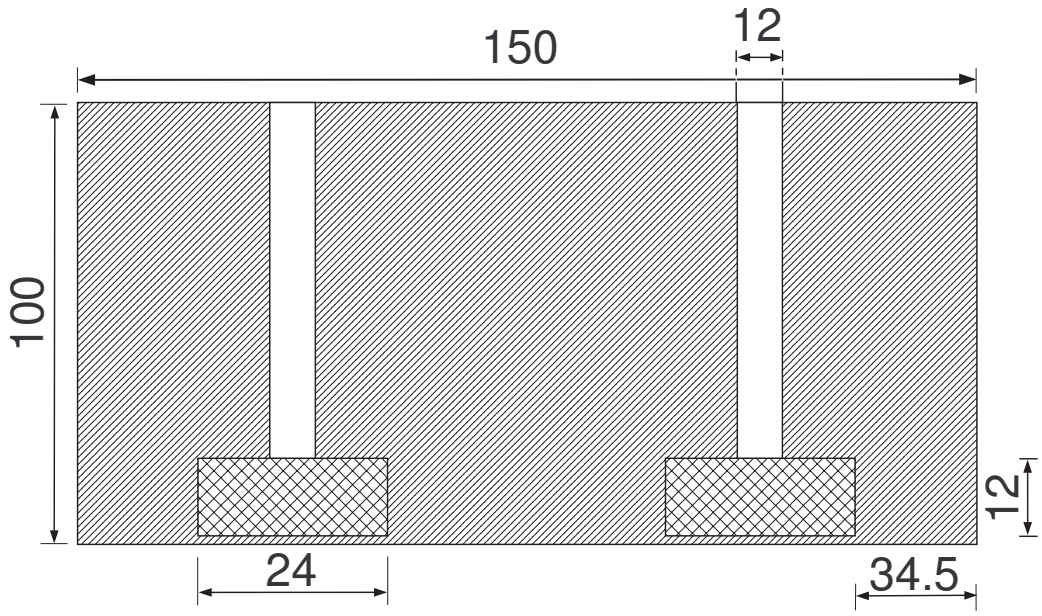

Figure E.4 Cross sectional Side View of 1 pole-pitch Vehicle

E.3 One and a Half Pole Pitch Vehicle

Figures E.5 and E.6 show the top view and side view of the $1^1/_2$ pole-pitch vehicle with dimensions.

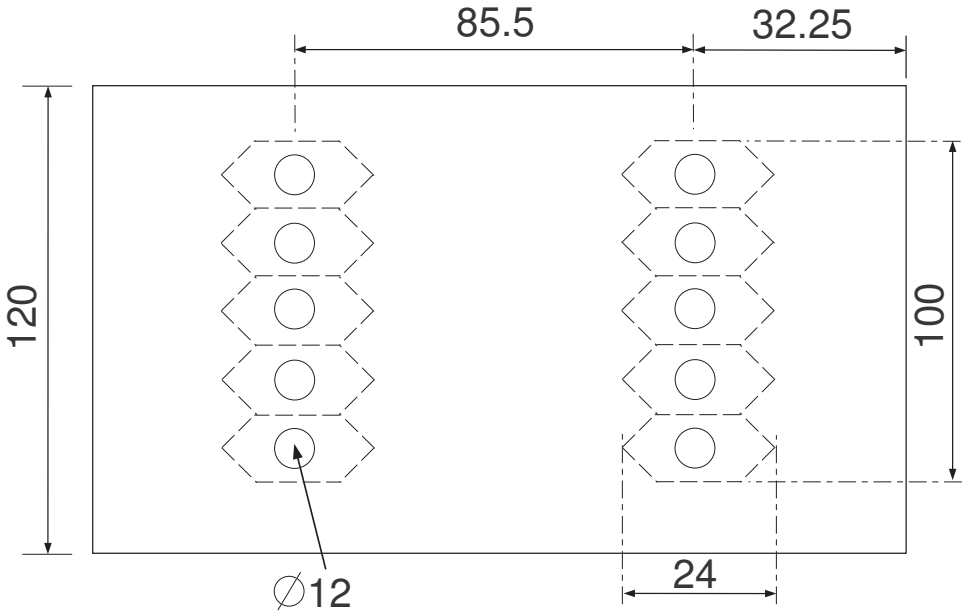

Figure E.5 Top View of $1^1/_2$ pole-pitch Vehicle

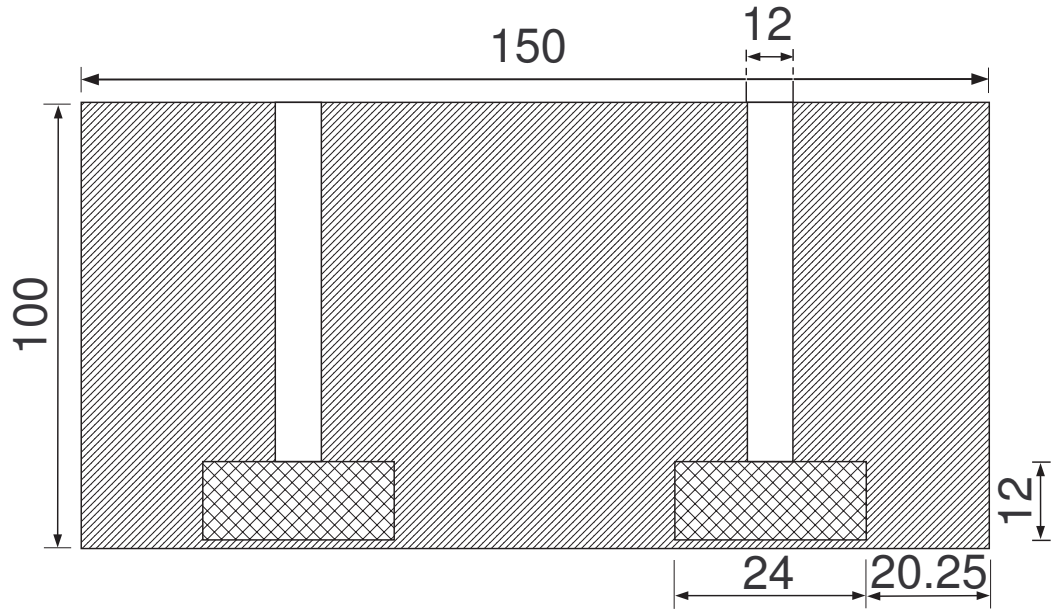

Figure E.6 Cross sectional Side View of $1^1/_2$ pole-pitch Vehicle